Theoretical studies as a tool for understanding the aromatic character of porphyrinoid compounds

Heike Fliegl,*[a] Rashid Valiev,[b] Fabio Pichierri[c] and Dage Sundholm*[d,e]

DOI: 10.1039/9781788010719-00001

1 Introduction

The scientific interest in porphyrinoid based materials is steady growing, since porphyrinoids are not only of biological relevance, but they also show interesting spectroscopic properties that link them to many possible applications such as near infrared dyes, photovoltaic dyes, field-effect transistors, nonlinear optical materials and nanoelectronic devices.[1–8] Biomedical applications of porphyrinoids are of particular importance specially for photomedical applications in cancer treatment, such as photodynamic therapy, multimodal imaging, drug delivery and biosensing.[9–12] Porphyrinoids show also an ability to form complexes with metals with unusual oxidation states and are therefore relevant for catalysis.[13–18]

The classic porphyrin molecule can formally be regarded as four pyrrole rings connected to each other by methin bridges.[19] Depending on the localization of the two inner pyrrolic hydrogen atoms the molecule is labeled *cis*- or *trans*-porphyrin. However, at room temperature the inner hydrogens generally move around inside the porphyrin ring.[20,21] The more general term porphyrinoids is used for a class of molecules that share the classical porphyrin structure for the macroring but differ for example by bearing various substituents or heteroatoms. Classic porphyrins, chlorins and bacteriochlorins are aromatic molecules satisfying Hückel's $(4n+2)$ π-electron count rule for aromaticity.[22,23] There is no doubt that aromaticity is an important concept in chemistry albeit it is still not fully understood and thus continuously under debate.[24–27] Theoretical calculations have shown that the aromatic pathways of

[a]*Hylleraas Centre for Quantum Molecular Sciences, Department of Chemistry, University of Oslo, P.O. Box 1033 Blindern, 0315 Oslo, Norway. E-mail: heike.fliegl@kjemi.uio.no*
[b]*Tomsk State University, Lenina 36, Tomsk, Russian Federation. E-mail: valievrashid@gmail.com*
[c]*Department of Applied Chemistry, Graduate School of Engineering, Tohoku University, Aoba-yama 6-6-07, Sendai 980-8579, Japan. E-mail: fabio@che.tohoku.ac.jp*
[d]*Department of Chemistry, P.O. Box 55 (A.I. Virtanens plats 1), FIN-00014 University of Helsinki, Helsinki, Finland. E-mail: dage.sundholm@helsinki.fi*
[e]*Centre for Advanced Study at the Norwegian Academy of Science and Letters, Drammensveien 78N-0271 Oslo, Norway*

classic porphyrins and porphyrinoids can differ, even though they have an almost the same degree of aromaticity.[28,29]

Structural modifications of porphyrinoids can be readily achieved experimentally by using organometallic approaches.[30] See for example different routes for synthesis of expanded porphyrins,[31–33] contracted porphyrins[34,35] and corroles[36] with aromatic as well as antiaromatic character. In particular, synthesis of Ni(II)–norcorrole has recently received attention, since it is air and water stable and is therefore a suitable cathode-active material in battery applications.[37] Antiaromatic Ni(II)–norcorrole shows an order of magnitude higher electrical conductance as compared to a similar aromatic Ni(II)–porphyrin complex, making the molecule highly attractive as component material for future molecular electronic devices.[38]

Experimental and computational studies show that aromatic pathways of non-classical porphyrins such as carbaporphyrins, where one pyrrolic nitrogen has been replaced by carbon and carbathiaporphyrins, where one pyrrolic nitrogen has been replaced by carbon and another one by sulfur, differ from that of classic porphyrins.[13,18,39–43] The existence of antiaromatic isophlorins was predicted by Woodward already in 1960[44] and synthesized in 2008 by Reddy and Anand.[45] Isophlorins are examples of air-stable antiaromatic porphyrinoids, which have been obtained by replacing an inner pyrrolic nitrogen atom by another heteroatom such as sulfur or oxygen.[45–48]

Considering the link between porphyrinoids and various applications of them, it is useful to have a deep understanding of their electronic structure and magnetic properties, in particular when aiming at a tailored design of porphyrin based materials with desired properties.[49–51] By controlling the number of π electrons that participate in the electron delocalization pathway, one can also adjust the electronic and spectroscopic properties of the porphyrinoids.[51,52] Through the control of the number of π electrons, the (anti)aromatic character and aromatic pathway can be tuned. However, the electron mobility pathways are not easily experimentally accessible, whereas calculated current densities provide accurate information about the current flow in the molecules when they are exposed to an external magnetic field.[41,42,53–55]

In the present review, we give a brief overview over different computational methods that are currently employed for assessing the degree of aromaticity of porphyrinoids with the main focus on current density calculations and studies performed by us and our coworkers. We decided to avoid the discussion of nucleus independent chemical shift (NICS) studies, because NICS studies have been recently reviewed.[56] However, some advantages and disadvantages of the NICS approaches are briefly discussed. Links between computational studies and experimental works are highlighted. The present review is structured as follows. A number of experimental methods motivating computational studies are briefly sketched in Section 2. In Section 3, we give an overview of some of the available theoretical methods that are used as aromaticity indicators. Recent applications on porphyrinoids and porphyrin based molecules are discussed in Section 4. An outlook is given in Section 5.

2 Experimental methods

Experimentally, aromaticity is related to energetic stabilizations, equalizations of bond lengths, preferred substitution reactions, and magnetic properties that differ from those of nonaromatic molecules.[57–69] Typical spectroscopic techniques that have been used for characterizing porphyrinoids are nuclear magnetic resonance (NMR),[70] ultraviolet (UV) absorption,[19,71,72] magnetic circular dichroism (MCD),[73,74] electronic circular dichroism (ECD),[75,76] photoelectron (PE),[77] two-photon absorption (TPA)[52,78,79] spectroscopies as well as cyclovoltametric (CV)[80,81] measurements to mention only the most commonly applied ones.

In the context of aromaticity studies, it is widely accepted that experimental proton nuclear magnetic resonance (^{1}H NMR) chemical shifts predict concordant degrees of aromaticity.[53,82–86] The ^{1}H NMR spectra show specific features such as a deshielding and downfield shift for the resonances of the protons that are attached to the exterior part of an aromatic ring.[87,88] The influence of the aromaticity on the ^{1}H NMR chemical shifts can be explained with the so called ring-current effect.[87–89] Ring shaped molecules such as porphyrins sustain magnetically induced currents when being exposed to an external magnetic field as it is the case for an NMR experiment. These ring currents generate an induced magnetic field that is oriented opposed to the external field in the case of an aromatic molecule. Typically, electrons that circle the classical (diatropic) direction are dominant in aromatic molecules, whereas the situation in antiaromatic molecules is reversed and ring currents that circle in the nonclassical (paratropic) direction dominate.[90] Albeit ring currents have not yet been measured directly they can indirectly be determined through measurements of ^{1}H NMR chemical shifts as pointed out above and by measuring magnetizabilities, see Section 3 for more details. Thus, computational aromaticity studies often adopt the magnetic criterion, since these properties are easier accessible and more robust as compared to estimates of aromatic stabilization energies (ASE) using a series of calculations of homodesmic reaction energies.[91–93] Knowledge of the pattern of magnetically induced currents leads to a deeper understanding of aromatic properties, which complements interpretations of experimental ^{1}H NMR spectra.[94–97] It is also possible to detect magnetic dipole electronic transitions between electronic states experimentally. Magnetically induced currents can in principle be detected in neutron scattering experiments.[98,99]

The UV/Vis absorption spectrum of porphyrins shows also characteristic features depending on their aromatic character. For example, the absorption spectrum of free-base porphyrin consists of weak Q_x and Q_y bands that appear in the red part of the visible region.[71] It has been shown theoretically that further peaks appearing in the Q-band region of the absorption spectrum of porphyrin are due to vibronic progression of $S_0 \rightarrow S_1$ and $S_0 \rightarrow S_2$ electronic transitions,[100] while the strong Soret B_x and B_y bands are typically broad peaks without any fine structure in the violet region.[19,71,101] The $S_0 \rightarrow S_1$–S_4 transitions of the classic porphyrins can be explained by employing Gouterman's four-orbitals model.[71] The

characteristic absorption features of free-base porphyrin can also be applied to other porphyrinoids. In this context one often refers to Soret-like and Q-like bands. While aromatic porphyrinoids have strong Soret-like bands and small Q-like bands, antiaromatic porphyrinoids can be identified by the ill-defined Soret-like bands and the absence of Q-like bands.[102,103]

In the past, magnetic circular dichroism (MCD) spectroscopy has proven to be very useful for assessing the Q bands of various porphyrinoids.[74,104,105] While the Soret bands are electric dipole allowed transitions, the Q bands are formally electric dipole forbidden and appear only weakly, even though the intensity of the Q bands are significantly enhanced by vibronic coupling effects of Herzberg–Teller type.[101] However, the transitions responsible for the Q bands are of HOMO to LUMO type, which implies a change in the orbital angular momentum that makes them detectable *via* MCD spectroscopy. Both Soret and Q bands are magnetic dipole allowed transitions and can be related to the Faraday B term in MCD theory.[74] MCD spectra depend on the aromatic or antiaromatic character of the porphyrinoid. For example, the negative-to-positive MCD signals around the Q and Soret bands are typical for aromatic porphyrinoids of lower molecular symmetry, while antiaromatic porphyrinoids show only very weak formally forbidden bands in the low energy region together with a clear Faraday B term.[103] Depending on whether the investigated porphyrinoid is aromatic or antiaromatic, the $(4n+2)$- or the $(4n)$-electron perimeter model developed by Michl *et al.* is a useful theoretical tool for estimating the shape of the MCD spectra at the four most prominent low-energy bands.[106–110] The relation between spectroscopic and structural properties of phthalocyanines based on frontier molecular orbital arguments has recently been reviewed[111] and will not be discussed further in the present review.

Two-photon absorption measurements (TPA) have also been used for assigning molecular aromaticity, because it is empirically known that larger TPA cross sections are observed for aromatic molecules as compared to their antiaromatic congener species.[52,112] Antiaromatic species are spectroscopically often characterized by broad absorption bands, very weak or no fluorescence activity, small TPA cross sections, ultrashort excited-state lifetimes, the presence of a low-lying optically dark state, and strong paratropic ring currents.[52,112,113]

3 Theoretical characterizations

There are numerous aromaticity indices and criteria available and discussing all of them is beyond the scope of the present review. Instead we give in Table 1 a brief overview of the most commonly applied criteria for assessing the aromatic character of general molecules and porphyrinoids. The aromaticity criteria is related to the π electron count of a molecule and it can be separated into energetic, geometric, magnetic, spectroscopic and optical criteria.

Table 1 Criteria for assessing the aromatic character. The table was inspired from ref. 117.

	Aromatic	Antiaromatic
π electron count	$(4n+2)$ Hückel	$(4n)$ Hückel
(Single twist)	$(4n)$ Möbius	$(4n+2)$ Möbius
(Double twist)	$(4n+2)$	$(4n)$
Energy	Stabilization	Destabilization
HOMO–LUMO gap	Large	Small
Bond lengths	Equalization	Alternation
HOMA	≈1	Very small, negative
Magnetizability	<0	<0 or >0
Anisotropy of diamagnetic susceptibility	Enhanced	Small
Susceptibility exaltation	High	Low
^{1}H NMR shifts	Diatropic (low field shift)	Paratropic (high field shift)
NICS	Large negative	Large positive
ACID	Closed surface	Closed surface
Current strength susceptibility	Large positive	Large negative
Current density	Closed diatropic Streamline loop	Closed paratropic Streamline loop
Bond magnetizability	Negative	Positive
UV spectra	High energy	Low energy
Soret-like bands	Strong	Ill defined
Electric dipole	Allowed	Allowed
Magnetic dipole	Allowed	Allowed
Q-like bands	Weak	Not present
Electric dipole	Forbidden	Forbidden
Magnetic dipole	Allowed	Allowed
MCD spectra		
Q band region	Negative to positive signal	No or weak signal
Soret band region	Negative to positive signal	Clear B term signal
PE detachment		
Energies	High	Low
TPA cross section	Large	Small

3.1 HOMA

A popular structural criterion for aromaticity is the bond-length alternation HOMA (harmonic oscillator model of aromaticity) index defined as[114]

$$\mathrm{HOMA} = 1 - \frac{\alpha_{CC}}{n}\sum_i \left(R_{CC,opt} - R_{CC,i}\right)^2 + \frac{\alpha_{CN}}{n}\sum_i \left(R_{CN,opt} - R_{CN,i}\right)^2. \quad (1)$$

The constants α_{CC}, α_{CN}, $R_{CC,opt}$, and $R_{CN,opt}$ can be found in ref. 114. The number of bonds forming the respective ring is labeled as n. As a rule, for aromatic rings with little bond-length alternation, the HOMA index is about 1, while very small and negative HOMA values indicate that the ring consists of localized single and double bonds implying that they are non- or antiaromatic.[114,115] Typically, the HOMA value is calculated along an anticipated delocalization pathway. However, the HOMA value is an indicative quantity and not a quantitative one, see for example ref. 116.

3.2 ACID

The anisotropy of the magnetically induced current-density tensor (ACID) method was initially developed for constructing a scalar function that can be used for computationally assessing the degree of electron delocalization in a molecule.[118,119] The ACID function is constructed using the anisotropic part of the current susceptibility tensor, which is also the key quantity in current density studies. The ACID function is a scalar function similar to the electron density having the advantage that it is independent of the direction of the external field and it is easy to visualize. However, the simplifications used for obtaining the ACID function come at the cost of loosing information by contracting the current density, which is a vector quantity. Another drawback is that ACID functions calculated using the commonly used implementation suffer from a very slow basis set convergence,[118] because ordinary basis functions are employed. The slow basis-set convergence affects the accuracy and reliability of the approach. Recently, Fliegl *et al.* implemented a method to calculate ACID functions using London orbitals in the GIMIC code.[120] The use of gauge-including atomic orbitals (GIAO) a.k.a London atomic orbitals (LAO) leads to a fast basis set convergence of the current density and consequently also of the ACID function. The GIAO-ACID method was tested on free-base *trans*-porphyrin. The isosurfaces of the ACID function for *trans*-porphyrin with two different isovalues are shown in Fig. 1 illustrating that visual inspection of the ACID function may lead to different interpretations regarding the electron mobility pathways depending on which isosurface is chosen.

3.3 NICS

ACID functions are often calculated in combination with nucleus independent chemical shift (NICS) values.[121,122] Current pathways in porphyrins have been investigated using this combination.[27] NICS values are obtained by placing a dummy atom (probe) in the center of a molecular

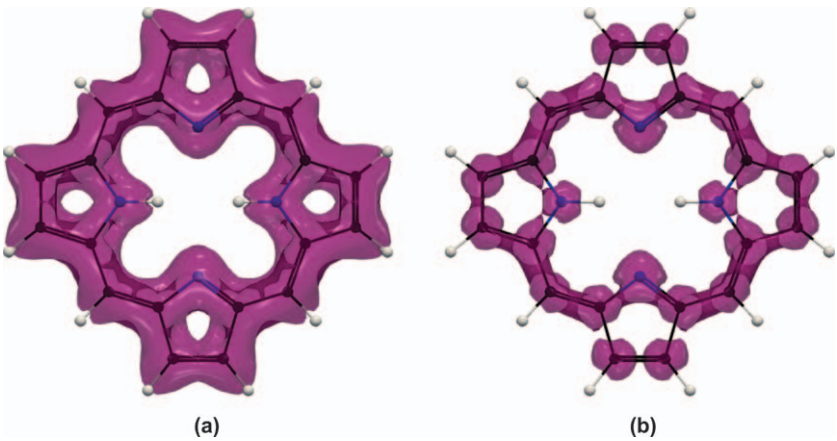

Fig. 1 The calculated ACID isosurface for *trans*-porphyrin plotted with isovalues of (a) 0.001 and (b) 0.005.

ring or above or below it. The negative isotropic shielding constant *i.e.* the magnetic response calculated in the probe is the NICS value. Several NICS approaches such as using the isotropic shielding constant or taking only the *zz* component of the shielding tensor into account are used. More sophisticated approaches such as calculating a set of NICS values along the symmetry axis of molecules or scanning the magnetic response in two or three dimensions are also employed.[56,123–129] It is a common misconception that NICS and current density calculations are identical approaches by referring to the Biot–Savart relation. A series of different studies has shown that current strength susceptibilities obtained from magnetic shielding data depend on the assumed current-pathway model. This explains why shielding based approaches lead to significant uncertainties in ring-current strength susceptibilities, current pathways, and consequently in the degree of aromaticity, specially when complicated molecules are investigated. This has been pointed out by several research groups.[90,122,123,125,130–136] Explicit current density calculations are more reliable as compared to NICS calculations. Calculated current densities provide deeper insights in particular when studying complicated ring systems.

3.4 Current density

When a molecule is exposed to an external magnetic field the electrons are forced to move, which is giving rise to the so called magnetically induced current density that induces a magnetic response. In case of aromatic molecules, the induced magnetic field is oriented in the opposite direction to the applied external field weakening the effect of the external magnetic field as in the classical case. For antiaromatic molecules, the induced magnetic field is aligned in the same direction as the applied one leading locally to a strengthening of the magnetic field.

In the framework of perturbation theory the magnetically induced current density can be expressed as a sum of diamagnetic $j_{\mathrm{m}}^{\mathrm{d}}$ and paramagnetic $j_{\mathrm{m}}^{\mathrm{p}}$ contributions[51,90,137]

$$j_{\mathrm{m}} = j_{\mathrm{m}}^{\mathrm{d}} + j_{\mathrm{m}}^{\mathrm{p}} = -\left(\frac{e^2}{m_{\mathrm{e}}}\right) A\psi_0^2 - i\left(\frac{e\hbar}{2m_{\mathrm{e}}}\right) \sum_{n\neq 0} (c_n - c_n^*)\left(\psi_n^{(0)} \nabla\psi_0 - \psi_0 \nabla\psi_n^{(0)}\right) \tag{2}$$

where e and m_{e} are the charge and mass of the electron, A is the vector potential needed to describe the external magnetic field and $\hbar$ is the Dirac constant. The unperturbed ground-state wave function is labeled ψ_0 and $\psi_n^{(0)}$ are unperturbed wave functions of the excited states. The expansion coefficients c_n of the first-order perturbed wave function in the basis of the unperturbed excited states are

$$c_n = \frac{\langle n|\hat{L}|0\rangle}{\Delta E_{n0}}. \tag{3}$$

Here, ΔE_{n0} denotes the energy difference between the nth electronic excited state and the ground state and $\hat{L}$ refers to the angular momentum

operator. The diamagnetic contribution to the current density is fully described by the ground-state wave function, while for calculating the paramagnetic part one needs to compute the matrix elements $\langle n|\hat{L}|0\rangle$, which formally involves excited state wave functions. Note, that only the total current density is physically meaningful. The expressions for the diamagnetic and paramagnetic contributions in eqn (2) depend on the chosen gauge origin.

3.5 GIMIC

The current density susceptibility tensor ($\mathscr{J}_{\gamma}^{\mathrm{B}_\beta}$) is related *via* the Biot–Savart law to the nuclear magnetic resonance (NMR) shielding tensor.[90] The elements of the magnetic shielding tensor for nucleus $I(\sigma_{\alpha\beta}^{I})$ can be written as

$$\sigma_{\alpha\beta}^{I} = -\varepsilon_{\alpha\delta\gamma}\int\frac{(r_\delta - R_{I\delta})}{|\mathbf{r}-\mathbf{R}_I|^3}\mathscr{J}_{\gamma}^{\mathrm{B}_\beta}\mathrm{d}\mathbf{r} \tag{4}$$

where $\varepsilon_{\alpha\beta\gamma}$ is the Levi–Civita tensor, $\mathbf{r}$ and $\mathbf{R}_I$ stand for electronic and nuclear coordinates. By combining the Biot–Savart relation and the analytic gradient expression for calculating NMR shielding tensors, one can derive an analytic expression for the current density susceptibility tensor as implemented in GIMIC program.[138,139] For closed-shell molecules the final expression for the tensor elements of the current density susceptibility reads

$$\begin{aligned}\mathscr{J}_{\upsilon}^{\mathrm{B}_\tau}(\mathbf{r}) = &\sum_{\mu\nu} D_{\mu\nu}\frac{\partial\chi_\mu^\star(\mathbf{r})}{\partial B_\tau}\frac{\partial\tilde{h}(\mathbf{r})}{\partial m_\upsilon^I}\chi_\nu(\mathbf{r}) + \sum_{\mu\nu} D_{\mu\nu}\chi_\mu^\star(\mathbf{r})\frac{\partial\tilde{h}(\mathbf{r})}{\partial m_\upsilon^I}\frac{\partial\chi_\nu(\mathbf{r})}{\partial B_\tau}\\ &+\sum_{\mu\nu}\frac{\partial D_{\mu\nu}}{\partial B_\tau}\chi_\mu^\star(\mathbf{r})\frac{\partial\tilde{h}(\mathbf{r})}{\partial m_\upsilon^I}\chi_\nu(\mathbf{r}) - \varepsilon_{\upsilon\tau\delta}\left[\sum_{\mu\nu} D_{\mu\nu}\chi_\mu^\star(\mathbf{r})\frac{\partial^2\tilde{h}(\mathbf{r})}{\partial m_\upsilon^I\partial B_\delta}\chi_\nu(\mathbf{r})\right]\end{aligned} \tag{5}$$

where $D_{\mu\nu}$ denotes the elements of the atomic orbital density matrix, B_τ the external magnetic field in the Cartesian direction $\tau = x,y,z$, $\chi_\mu(\mathbf{r})$ are Gaussian type basis functions and m_υ^I are the vector components of the magnetic moment of nucleus I. The use of gauge including atomic orbitals (GIAO) a.k.a. London atomic orbitals (LAO) leads to gauge origin independence of the calculated current densities and a fast basis-set convergence.[138] The calculated current density does not have any reference to the nuclear positions, even though the magnetic interaction with magnetic moments appears in eqn (5). The expression for the one-electron magnetic interaction Hamiltonian $\tilde{h}$ is given in more detail in ref. 51 and 138. The GIMIC method has also been generalized to open-shell molecules.[139]

Contraction of the current density susceptibility tensor with the external magnetic field leads to a gauge-origin independent expression for the magnetically induced current density corresponding to the one in

eqn (2). The current density for a given direction of the external magnetic field is a vector quantity. The calculated current density is usually visualized in a plane placed one bohr above the molecular plane. It can be represented as a vector plot or with streamlines[140] that follow the trace of an infinitesimal small particle flow along the direction of the vector field[51] as shown for *trans*-porphyrin in Fig. 2. Very fine streamlines can be visualized using the line integral convolution technique (LIC) as implemented in ParaView.[141] Visual inspections of current density maps are indeed helpful. However, as we show in Section 4 current density plots are not enough and should always be supported by an integration analysis, because solely plotting the current flow in selected planes may lead to wrong conclusions about the dominating current density flow.[28,51]

GIMIC is an independent program that is freely available.[142] It needs basis-set data as well as the magnetically perturbed density matrices and the ordinary density matrix in atomic orbital basis as input information. This information is provided by an electronic structure code when performing for example nuclear magnetic shielding calculations. GIMIC has been interfaced to a number electronic structure codes. Calculations of the current density using gimic are independent of the level of theory, because electron correlation effects are included in the density matrices when a correlated level is employed in the nuclear magnetic shielding calculation. A key feature of GIMIC is its ability to perform integrations of the current flow across selected chemical bonds leading to quantitative information about the current flow. The resulting quantity is referred to as the *integrated current strength susceptibility*. It was recently shown that there is a linear relation between ring current strength susceptibilities and hydrogenation enthalpies for assessing the degree of aromaticity.[143]

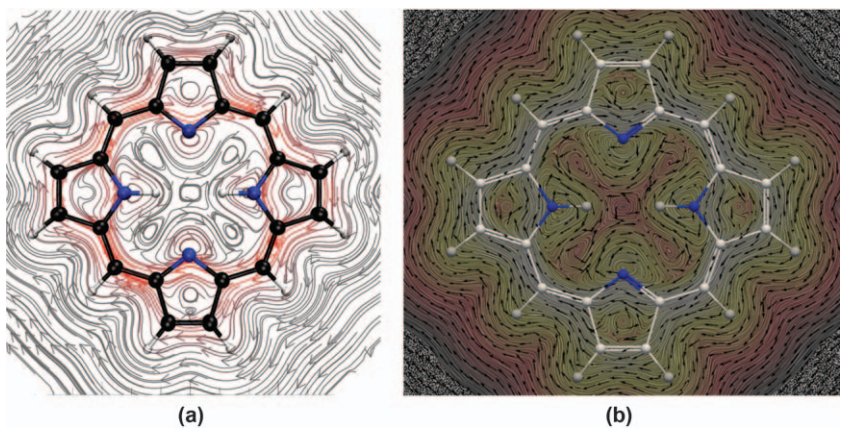

Fig. 2 The calculated current density susceptibility for *trans*-porphyrin in a plane placed 1 bohr above the molecular plane. The current density is represented using (a) a streamline plot with stronger current streams shown in red and (b) a line integral convolution (LIC) streamline plot including arrows. Diatropic currents are assumed to circle clockwise.

3.6 Magnetizability

When discussing magnetizabilities one often refers to the experimentally measurable bulk quantity as *magnetic susceptibility* and to the molecular property as *magnetizability*.[144] The magnetizability χ_m of a molecule is defined as the second derivative of its ground-state energy E with respect to the external magnetic field B,

$$\chi_m = -\mu_0 \frac{d^2E}{d\mathbf{B}^2}, \tag{6}$$

where μ_0 is the vacuum permeability. As the magnetically induced current density the magnetizability can be expressed as a sum of its diamagnetic (χ_m^d) and paramagnetic (χ_m^p) contributions[137]

$$\chi_m = \chi_m^d + \chi_m^p = -\left(\frac{e^2\mu_0 N_A}{6m_e}\right)\langle r^2\rangle + \left(\frac{e^2\mu_0 N_A}{6m_e}\right)\sum_{n\neq 0}\frac{|\langle n|\hat{L}|0\rangle|^2}{\Delta E_{n0}} \tag{7}$$

where N_A is Avogadro's constant. The division of the magnetizability into diamagnetic and paramagnetic contributions depends on the chosen gauge origin. The largest contributions to the paramagnetic term χ_m^p are expected from the lowest excited electronic states, because of the small energy denominator. The magnetizability and the current density susceptibility are related in the following manner:[90]

$$\chi_{\alpha\delta} = \frac{1}{2c}\varepsilon_{\alpha\beta\gamma}\int d\mathbf{r} A_\beta \mathscr{J}_\gamma^{B_\delta}(\mathbf{r}). \tag{8}$$

The magnetizability can be obtained by performing a three-dimensional integration of the current density susceptibility multiplied with the vector potential ($A_\beta = x,y,z$) of the external magnetic field.[90] By using the theory of atoms in molecules, Bader and Keith showed that the magnetizability can be estimated by adding atomic or group contributions.[145] The same procedure was earlier proposed by Pascal and Pacault.[146–148] Based on this idea, the intra-atomic or bond magnetizability concept was introduced.[145]

3.7 The gauge problem

The magnetizability cannot be uniquely divided into paramagnetic and diamagnetic contributions even when one uses GIAOs,[149] because this property depends on the direction of the magnetic field, the gauge origin of the magnetic field, and the origin of the Cartesian coordinate system. After evaluating the atomic integrals, the gauge origin vanishes, but the dependence on the origin of the Cartesian coordinate system remains. Thus, the individual contributions to the total magnetizability depend on the Cartesian origin even though the total magnetizability is unaffected by shifting the origin.[149] The magnetizability is usually divided into a diamagnetic part that depends only on the ground-state wave function and a paramagnetic contribution that comprises the response terms due to the applied external magnetic field.[90]

The diatropic and paratropic current density flows can be defined with respect to a chosen coordinate origin. For example, by choosing the origin at the center of a molecular ring one can determine whether the ring current of the studied ring is diatropic or paratropic *i.e.*, if the current density circulates around the ring in the classical or non-classical direction, respectively. However, a diatropic current density flow of the studied ring will be paratropic with respect to the center of an adjacent ring.

3.8 Magnetic transitions in electronic spectra

A magnetic-dipole electronic transition between an initial electronic state $|0\rangle$ and a final state $|n\rangle$ can be expressed as matrix elements over the magnetic dipole operator $\hat{M}$

$$M_{n0} = \langle n|\hat{M}|0\rangle \quad \text{with} \quad \hat{M} = \mu_B(\hat{L} + g_e\hat{S}) \tag{9}$$

where μ_B is the Bohr magneton, g_e is the electronic g-factor, $\hat{L}$ is the angular momentum operator and $\hat{S}$ is the electronic spin operator. If one considers only closed-shell molecules, the matrix elements over $\hat{S}$ vanish and the remaining matrix elements that contain the angular momentum operator $L_{n0} = \langle n|\hat{L}|0\rangle$ contribute to the magnetic-dipole transition $S_0 \rightarrow S_n$.

As seen in the previous sections the key quantities for investigating magnetic and optical properties are matrix elements over the angular momentum operator. This operator connects in a sense magnetically induced current densities, magnetic dipole transitions and magnetizabilities, because calculations of these quantities involve the same matrix elements over the angular momentum operator ($\hat{L}$). It is very likely that there is also a relation between the rotational strengths of magnetical circular dichroism (MCD)[73] spectra and magnetically induced current densities since both quantities share expressions over the angular momentum operator. MCD spectroscopy on porphyrinoids has been discussed in detail by Mack *et al.* in ref. 74.

4 Applications

Aromaticity and aromatic pathways of classic porphyrins have been computationally studied by several research groups.[28,115,126,150–160] Noteworthy are for example current density maps studies using the ipsocentric CTOCD-DZ method to determine current pathways in porphyrins.[152,159,161–163] The ipsocentric CTOCD-DZ method relies on ordinary perturbation-independent basis sets. The CTOCD-DZ method is constructed to yield gauge-independent current densities, whereas large basis sets have to be used when calculating current strengths, because ordinary basis sets rather than perturbation-dependent GIAOs are employed.[164] The current densities obtained in CTOCD-DZ calculations can be decomposed into orbital contributions,[165] which has not been done in the GIMIC approach. Presently, the most reliable approach for assigning the aromatic character of molecules according to the magnetic

criterion is by investigating magnetically induced current densities.[28,51,54,166,167]

In the following, we highlight current density applications starting with classical porphyrin systems such as *trans*-porphyrin. Then we look at the influence of different substitution patterns such as replacing an inner pyrrolic nitrogen with other atoms followed by N-confusion and insertion of different rings such as thiophene. Finally, we turn our attention to metal containing porphyrins, porphyrin arrays, contracted porphyrins, and expanded singly and doubly twisted porphyrins.

4.1 Classical porphyrins

Free-base porphyrin, chlorin and bacteriochlorin belong to the group of classical porphyrins. The chlorins share the core porphyrin structure but due to the saturated C_β–C_β bonds of the pyrrolic ring, the current pathways and current strength susceptibilities differ.[28] In Fig. 2, the molecular structure of *trans*-porphyrin is shown together with the calculated current density illustrated using two different streamline visualization techniques. Independent on the choice of visualization, one clearly sees that the ring current is divided at each subring suggesting that the single pyrrolic rings do not sustain any significant local ring current. However, visualization only, independent of its level of sophistication, is not enough to obtain a clear picture of the underlying current pathways, since one might easily reach the incorrect conclusion that the 18π electron delocalization pathway is the favored one. Fliegl and Sundholm showed that an additional integration analysis of the current density is mandatory for providing reliable current pathways.[28] This integration analysis introduced a new viewpoint regarding the ongoing dispute whether the 18π [18]annulene picture,[17,151,168–170] which assumes that the inner NH groups act as inert bridges, or the newer 18π [16]annulene inner cross route[115,156,171] provides the correct description of the aromatic pathway of porphyrins.

The current strength susceptibilities obtained in the numerical integration are given in Table 2. For comparison, the table also includes integrated values for the ACID cross section area for *trans*-porphyrin showing that in this case both methods lead to roughly the same conclusion.[120] Only a visual inspection of the ACID surface would support the 18π [18]annulene picture for the current pathway. The integrated

Table 2 Integrated current strength susceptibility J (in nA/T) and the ACID cross-section area $|\Delta\mathscr{J}^2|^{\frac{1}{2}}$ (in nA/T) for free-base *trans*-porphyrin. Pyrrolic rings with inner hydrogens are denoted by the superscript ^{H}. The numerical integrations were performed at the center of the chemical bonds. The current density as well as the ACID cross-section area were calculated at the B3LYP/TZVP level. Grid-point spacings of 0.02 were used in the numerical integrations, see ref. 120.

	C=C		C–N–C		Total	
Ring	J	$\lvert\Delta\mathscr{J}^2\rvert^{\frac{1}{2}}$	J	$\lvert\Delta\mathscr{J}^2\rvert^{\frac{1}{2}}$	J	$\lvert\Delta\mathscr{J}^2\rvert^{\frac{1}{2}}$
A^H	18.5	4.0	8.7	3.4	27.2	7.4
B	12.3	2.9	15.2	4.4	27.5	7.3

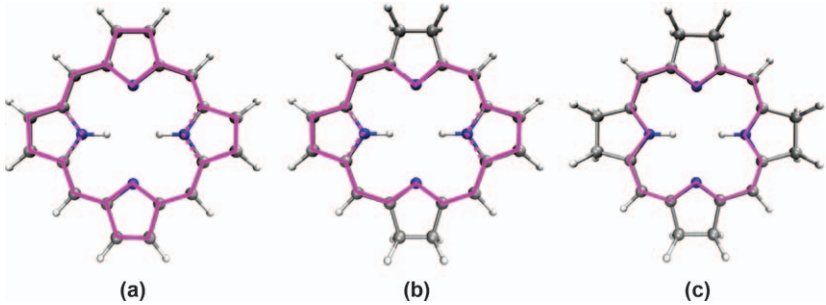

Fig. 3 Schematic overview over the strongest current pathways that are indicated in pink for (a) *trans*-porphyrin, (b) bacteriochlorin and (c) fully β-saturated porphin, see ref. 28.

current strength susceptibilities confirm that the current indeed divides into two pathways at each pyrrolic ring. At ring B, that has no inner hydrogen, the ring current flows almost equally along the inner and the outer pathways, whereas at ring A the current flow along the outer route *via* the C=C bond is 10 nA/T stronger than the current passing the inner NH moiety. The net current strength of 8.7 nA/T passing the NH moiety is not negligible. Thus, one can conclude that the 18π [18]annulene electron pathway is not the correct picture for *trans*-porphyrin. The 18π [16]annulene interpretation can also be ruled out, because strong currents of 18.5 nA/T and 12.3 nA/T pass the outer C=C bond indicating that all 26 π electrons of free-base porphyrin participate in the electron delocalization pathway. There is no evidence that the pyrrolic rings sustain any strong local currents.[51]

Using the integration procedure described above leads to information about the preferred current pathways within a molecule when it is exposed to an external magnetic field. It has been shown that systematic hydrogenation of the pyrrolic rings can be used to force an 18π [18]annulene or 18π [16]annulene current pathway upon a porphyrin based molecule.[28] Fig. 3 gives a schematic overview of the different pathways obtained upon saturating the $C_\beta = C_\beta$ double bond of the pyrrolic rings.

4.2 Aromaticity of porphyrins

The aromatic character of porphyrins can be understood by considering that they are planar molecules with approximately circular symmetry. Thus, in the aufbau of the many-body wave function one can assume that the π orbitals consist of a radial function multiplied with the angular function $\exp(\mathrm{i}m\varphi)$, where m is the azimuthal quantum number for rotation φ around the symmetry axis at the ring center. In this picture, the two energetically lowest π electrons occupy the total symmetric orbital corresponding to $m = 0$. The energetically higher-lying π orbitals with $\pm m$ and $m \geq 1$ are pair-wise degenerate hosting four electrons. Porphyrins with $4n + 2$ π electrons are then aromatic closed-shell molecules, whereas antiaromatic porphyrins have the energetically highest m shell half-filled with the electrons coupled to a singlet. When they couple to a triplet, the two orbitals of the m shell must be occupied by one electron each, leading to closed shells for the spin-up electrons and for

the spin-down electrons, which explains why the triplet state of molecules with $4n$ π electrons is aromatic.[172]

4.3 Heteroporphyrins

The porphyrin core can be modified by replacing the nitrogen of the pyrrolic rings with sulfur and oxygen, which can be considered to be isoelectronic with the NH moiety. The same idea can also be applied to carbon, because CH is isoelectronic with N and CH_2 is isoelectronic with NH. In porphyrins, the nitrogens of the pyrrolic rings are located inside the macroring, whereas also porphyrins with nitrogens located at the outer edge have been synthesized. The modifications of the porphyrin core yield heteroporphyrins such as true carbaporphyrins with one of the pyrrolic rings replaced by a five-membered all-carbon ring and N-confused porphyrinoids with an inverted pyrrolic ring.[13,40] The magnetically induced current densities have been calculated for a number of heteroporphyrins showing that it is hard to determine the current pathways using experimental data.[41,42,160] Explicit current density calculations are recommended when aiming at a detailed picture of the aromatic pathways in heteroporphyrins.

Isophlorins are strongly antiaromatic porphyrinoids that have heteroatoms such as oxygen and sulfur instead of nitrogen.[45,46,48] They are difficult to synthesize, because they easily oxidize forming aromatic porphyrinoids. Isophlorins that are considered to have a 20 π electron pathway were predicted already in 1960 by Woodward.[44] In 2008, air stable tetraoxa isophlorin and dioxa-dithia isophlorin were synthesized.[173] A current density investigation of these molecules confirmed that they are indeed strongly antiaromatic with ring current strengths of -50 nA/T to -60 nA/T. Fig. 4 shows the preferred current pathway for pentafluorophenyl substituted dioxa-dithia isophlorin. The calculated integrated current strength susceptibilities for selected bonds are also given illustrating on how the currents flow around the isophlorins. The paratropic ring current also divides into outer and inner pathways at the furan and thiophene rings. The pentafluorophenyl substituents are oriented perpendicular to the porphyrinoid macroring. They reduce the ring current strength by only 4–6 nA/T by slightly reducing the electron charge of the isophlorin ring.

The calculated and measured ^{1}H NMR chemical shifts differ suggesting that the isophlorins are less antiaromatic under experimental conditions as compared to a single molecule in vacuum. The current density analysis indicates that the strongest paratropic currents circle within the porphyrinoid macroring. Thus, one can assume that the ^{1}H NMR chemical shifts of the hydrogens at the β carbons depend linearly on the ring current strength of the porphyrinoid macroring. Following this assumption ring current strengths of -25 nA/T to -30 nA/T have been estimated for the isophlorins under experimental conditions.[53] More recent calculations on antiaromatic porphyrinoids showed that the B3LYP functional yields too strong paratropic ring current susceptibilities of strongly antiaromatic molecules.[174] Calculations at the second-order Møller-Plesset

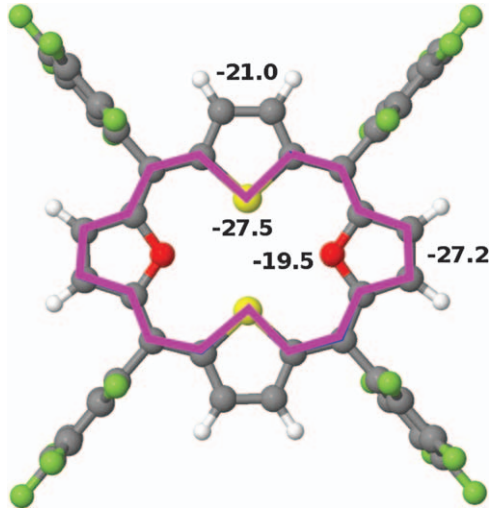

Fig. 4 The calculated ring current strengths (in nA/T) for pentafluorophenyl substituted dioxa-dithia isophlorin. The strongest current pathway is indicated with the pink line.[53]

perturbation theory level and at the DFT level using the BP97-D functional[175] yielded weaker current strengths that agree well with those estimated from the ^{1}H NMR chemical shifts.[174] Nevertheless, the studied isophlorins are very antiaromatic molecules.

Another possible modification of the *trans*-porphyrin core structure is to replace one pyrrolic nitrogen atom with an isoelectronic CH moiety leading to a new class of molecules that is called carbaporphyrins.[13] Carbaporphyrins were already predicted to exist in the 1940th by Aronoff, Calvin and Pauling[14,15] but it took more than 50 years until the first one was synthesized.[16,17] Berlicka *et al.*, Szyszko *et al.* and Lash *et al.* have more recently synthesized a variety of carba- and carbathiaporphyrins including metal complexes.[13,40,176–178] The term carbathiaporphyrin labels a carbaporphyrin where another pyrrolic nitrogen has been replaced by sulfur. Fig. 5a and b show the molecular structures of carbaporphyrin and carbathiaporphyrin, respectively. Carbathiachlorin with one C = C double bond of the cyclopentadienyl ring being saturated is shown in Fig. 5c. The calculated current pathways[41] are indicated with black arrows and the current strength susceptibilities are reported. The calculations show that replacing N with a CH moiety leads to a change in the current pathway such that the current strength of the inner route of the all carbon ring of 20.5 nA/T is much stronger than the one for the outer route of 6.3 nA/T. The current pathway changes significantly when replacing the opposite NH moiety with S. Then, most of the current takes the outer pathway at the pentadienyl ring and at the thiophene ring almost all the current flow goes *via* the sulfur. Saturation of the C_{β}–C_{β} bond of the all-carbon ring forces the current to inner route over CH, which also leads to a change in the current flow at the thiophene ring where most of the current passes along the outer pathway.[41] The underlying reason for the change in the current flow is not yet completely

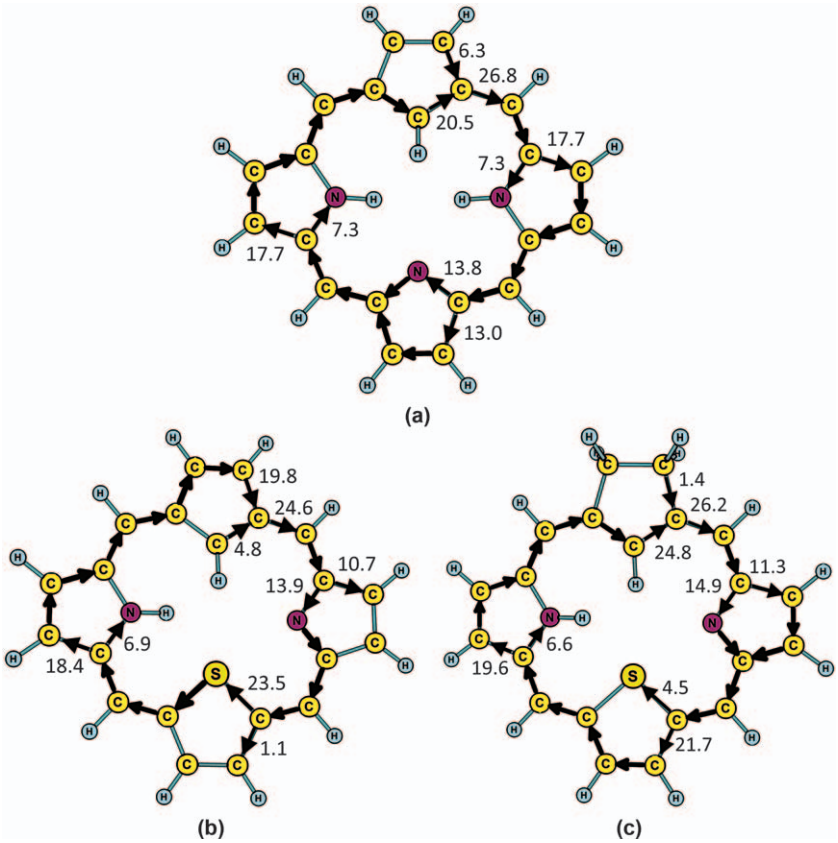

Fig. 5 The calculated ring current strength susceptibilities (in nA/T) for (a) carbaporphyrin, (b) carbathiaporphyrin and (c) carbathiachlorin.[41] The current pathway are indicated with black arrows.

understood. A possible explanation might be that the system wants to keep a current flow that can be written as a linear combination of aromatic $(4n+2)$ π electron pathways. The strength of the outer pathway in the pyrrolic ring without an inner hydrogen is 11.3 nA/T, which is equal to the sum of the current strengths passing the sulfur and NH moieties. Thus, the current flow can be written as a linear combination of three 18 π-electron pathways, where two take the outer routes at the pyrrolic ring without an inner hydrogen and inner routes at S or NH, respectively. The third one takes the inner pathway at the pyrrolic ring without an inner hydrogen and the outer pathway at the two other five-membered rings with an unsaturated C_β–C_β bond. Insertion of inner CH_2 groups cut the flow of diatropic currents, whereas in strongly antiaromatic molecules a significant fraction of the paratropic ring-current is still able to pass the sp^3 hybridized inner carbon atoms.[42]

A further alternative for modifying the porphyrin core structure is to invert one or several pyrrolic rings leading to compounds called N-confused porphyrins, which also belong to the class of carbaporphyrins.[18,179] Carbaporphyrinoids consisting of at least one all-carbon ring are often

distinguished from N-confused porphyrins by using the prefix *true* in front of the name of the carbaporphyrin. Current density studies on N-confused porphyrins showed that single N-confusion leads to a decrease in the aromatic character from 27 nA/T, which is the net current strength susceptibility of *trans*-porphyrin, to 16.4 nA/T, while inversion of the second pyrrolic rings had a smaller effect leading to ring current strengths of 13–14 nA/T.[42]

4.4 Porphyrinoids with fused rings

In this subsection, we discuss current density studies of porphyrinoids with fused rings that exhibit very complicated current patterns. All molecules highlighted here are exceptional in the sense that they contain fused rings with a current flow of the opposite tropicity as compared to the tropicity of the macroring.

2,3-thieno-bridged and 3,4-thieno-bridged porphyrin are porphyrinoids consisting of a thiophene ring fused to free-base porphyrin. The annelated thiophene ring is fused to the porphyrin ring between the β carbon of the pyrrolic ring and the meta carbon of the porphyrin ring forming a five-membered carbon ring between the thiophene ring and the porphyrin. The two molecules shown in Fig. 6 differ by the orientation of the thiophene ring.

The two isomers have been synthesized by Mitsushige *et al.*[180] who reported different spectroscopic properties for the molecules with different orientations of the thiophene ring. They concluded that the 2,3-thieno-bridged porphyrin formally consisting of a 20 π-electron aromatic pathway is characterized by a stronger antiaromatic contribution than the 3,4-thieno-bridged porphyrin, which formally consists of a 24 π-electron aromatic pathway.[180] The main conclusion drawn from the spectroscopic data was that the aromaticity of thieno-bridged porphyrins can be divided into global aromatic and antiaromatic contributions, whose mutual extent can be controlled by the direction of the annelated thiophene ring, which means that the compounds might serve as an aromatic switch. However, Mitsushige *et al.* were not able to trace back the underlying reason for the different antiaromatic contributions of the molecules based on the available experimental and theoretical data.[180]

We studied the current densities of the 2,3-thieno-bridged and 3,4-thieno-bridged porphyrins.[181] The calculated current densities in Fig. 6 indicate that both molecules are aromatic. An analysis of the current density yielded a deeper understanding of the underlying reason for the different aromatic character and the degree of aromaticity of the two molecules.[181] The five-membered ring between the thiophene and porphyrin rings sustains a much stronger paratropic ring current in 2,3-thieno-bridged porphyrin than in 3,4-thieno-bridged porphyrin, which can be traced back to the orientation of the thiophene ring. The bond-length alternation of the thiophene ring leads to a stronger bond length alternation of the five-membered ring between the thiophene and the porphyrin in 2,3-thieno-bridged porphyrin than in the 3,4-thieno-bridged

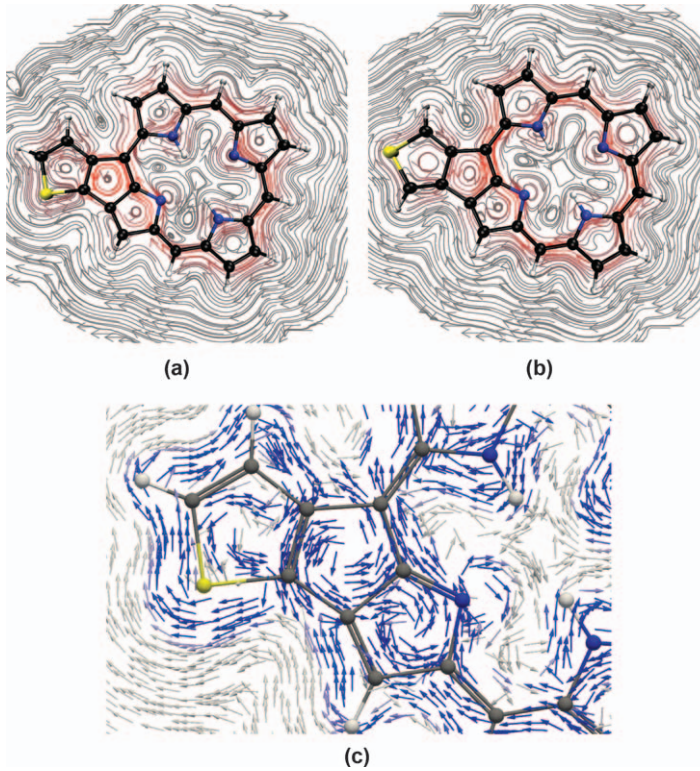

Fig. 6 The calculated current density in a plane 1 bohr above the molecular plane is shown using streamlines. The current densities for (a) 2,3-thieno-bridged porphyrin and (b) 3,4-thieno-bridged porphyrin are depicted. Stronger currents are highlighted in red. (c) The current density for 2,3-thieno-bridged porphyrin is visualized using arrows. Blue arrows indicate stronger currents. The zoomed view of the three connected rings shows that the five membered as well as the pyrrolic ring sustain a paratropic current albeit the current flow around the macroring is diatropic. Diatropic currents are assumed to circle clockwise, paratropic ones anti-clockwise.

porphyrin. Thus, according to the harmonic oscillator model of aromaticity (HOMA),[114] one can expect a stronger antiaromaticity of the five-membered ring of the 2,3-thieno-bridged porphyrin than for the 3,4-thieno-bridged porphyrin. Our current strength susceptibility analysis shows that the change in the orientation of the thiophene ring is not enough to switch the aromatic character of the whole porphyrinoid macroring. The net current strength of the 2,3-thieno-bridged porphyrin is 16.2 nA/T as compared to 22.8 nA/T for the 3,4-thieno-bridged porphyrin.[181] The strong paratropic ring current flowing around the five-membered ring influences the neighboring pyrrolic ring, which also sustains a paratropic ring current. A stronger paratropic ring current in the five-membered ring leads to a stronger paratropic ring current in the pyrrolic ring. The antiaromatic rings are zoomed in Fig. 6c. The diatropic ring current of the porphyrinoid macroring is forced to take the inner route at the antiaromatic pyrrolic ring. The orientation of the thiophene ring determines the strength of the paratropic ring current in the five-membered ring, which affects the strength of the paratropic ring current

of the pyrrolic rings and the strength of the diatropic ring current of the porphyrinoid macroring.[181]

The current density has also been studied for antiaromatic porphyrinoids with formally $4n$ π electrons such as thienopyrrole core-modified porphyrinoids,[54] where one of the pyrrole rings is replaced by a thienopyrrole moiety. The calculated current density of the tautomer 1-3 of the thienopyrrole core-modified porphyrinoid is shown in Fig. 7,[54] representing the recently synthesized thienopyrrole core-modified porphyrinoid structures.[182] Tautomer 1-3 is strongly antiaromatic sustaining a ring current of −50.0 nA/T. The pyrrolic ring annelated to the thiophene ring has a very strong diatropic current flow as illustrated Fig. 7c. The current density study showed that ethyl-formate substitution leads to a weakening of the net current strength of the macroring. For tautomer 2-4, which is the energetically lowest tautomer, the ethyl-formate substitution leads to a change of the aromatic character of the porphyrinoid macroring from antiaromatic (−11.7 nA/T) to nonaromatic (−0.4 nA/T), whereas alkyl substitutions did not affect the ring current strength significantly. The hydrogen of the pyrrolic ring annelated to the thiophene ring forms a hydrogen bond with the lone electron pair of the oxygen of

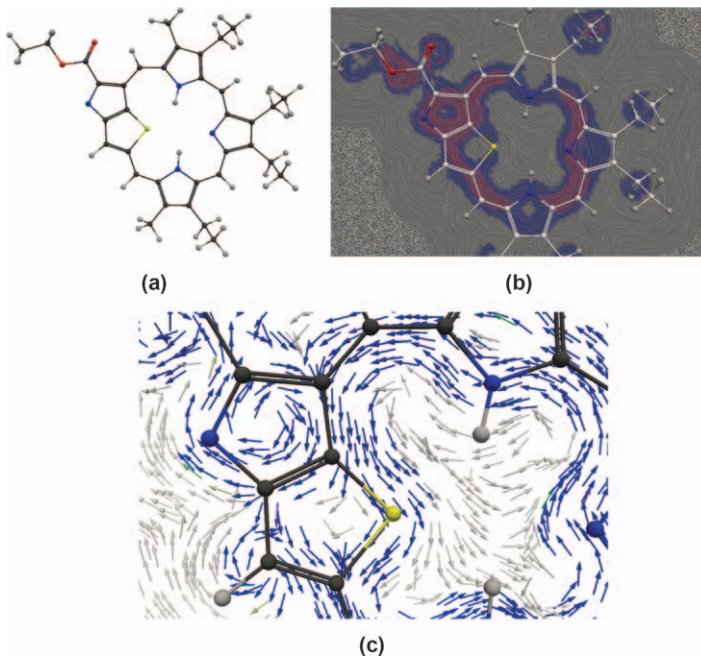

Fig. 7 (a) The structure of the antiaromatic 1-3 tautomer of the thienopyrrole modified porphyrin reported in ref. 54 (b) The calculated magnetically induced current density of the 1-3 tautomer represented as LIC streamlines. The current density is calculated in a plane 1 bohr above the molecular plane. Stronger currents are highlighted in pink and blue is used for highlighting the global ring current. (c) A strong local diatropic ring current is sustained by the pyrrolic ring as seen in the zoomed picture. In (c), the current density is visualized using arrows. Blue arrows indicate stronger currents and grey arrows represent weaker ones.

the carboxyl group, which stabilizes the molecule and destroys the antiaromatic character of the porphyrinoid ring.

We also investigated the aromatic character of a number of traditional and modified carbaporphyrinoids such as oxybenziporphyrin,[183–185] benzocarbaporphyrin,[186,187] azuliporphyrin,[186,188,189] tropiporphyrin[190,191] and carbachlorins[192] using calculations of magnetically induced current densities at the DFT level.[43] Fig. 8 shows tropioporphyrin as an illustrative example for a fused cycloheptatrienyl ring to a porphyrinoid macrocycle. The net current strength of tropiporphyrin is 22.1 nA/T, which is 82% of the ring-current strength of carbaporphyrin, thus the molecule is aromatic according to the ring current criterion. The ring current flowing around the macrocycle preferably takes the outer routes at the pyrrolic rings. The fused cycloheptatrienyl ring is with a current strength of −15.9 nA/T antiaromatic sustaining a strong local paratropic ring current. The opposite current flow at the cycloheptatrienyl ring is visualized in Fig. 8a and b using an arrow representation for the current density calculated in a plane placed 1 bohr above the molecular plane. Fig. 8c shows the calculated current strength susceptibility for selected bonds. In the case of tropioporphyrin, a strongly antiaromatic ring is annelated to an aromatic one,[43] which is similar to the thienopyrrole modified 20 π-electron porphyrinoids and the thienobridged porphyrin molecules discussed above.[54,181]

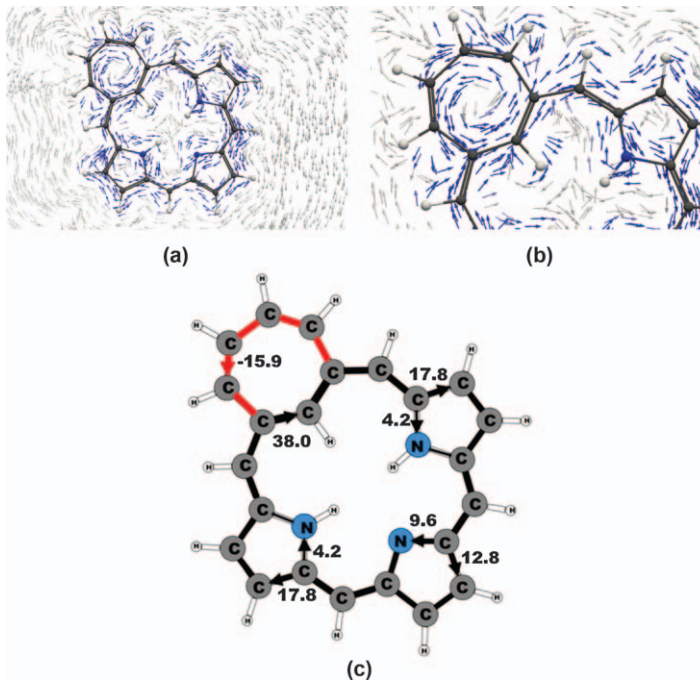

Fig. 8 The calculated current density of tropioporphyrin using a vector representation (a) visualized in a plane placed 1 bohr above the molecular plane. Stronger currents are highlighted as blue arrows. (b) The zoomed view illustrates the different current flow at the seven-membered ring. (c) The integrated current strength susceptibility for selected bonds. Reproduced from ref. 43 with permission from The Royal Society of Chemistry.

4.5 Metal containing porphyrins

Only a few current density studies of metal containing porphyrins have been published. One reason is that the integration analysis of the current density becomes more demanding, since currents passing across the metal center require denser integration planes and it is difficult to avoid current contributions from neighboring moieties that affect obtained current strengths. The electronic structure of transition metal containing compounds has often a multiconfiguration character implying that NMR shielding calculations that provide the necessary input data for calculating the current density are demanding.

Effective core potentials (ECP) are employed for considering relativistic effects due to heavy elements in the molecule.[193,194] The ECP replaces the core electrons and affects the current density. However, mainly atomic currents around the heavy element are reduced by the use of ECPs, whereas the current density of the valence electrons is assumed to be more or less the same as in the corresponding all-electron calculation.[195] Current density calculations have also been performed at fully relativistic levels.[196–198] However, four-component calculations are computationally expensive limiting applications to rather small systems.

Current density calculations have been performed on porphyrinoid complexes with Zn^{2+} and Ni^{2+}, which are d^{10} and d^{8} species that behave differently. Zn^{2+} with the closed d shell is rather inert, behaving in the same way as Mg^{2+}, whereas Ni^{2+} was found to play a more active role in the current density of Ni(II)–norcorrole.

The antiaromatic Zn(II)–octaethylporphyrin (Zn–OEP) cation was obtained by oxidizing neutral Zn–OEP with $AgSbF_6$ and I_2.[199] Current density calculations yielded a ring current strength of −51.7 nA/T, whereas a comparison of the calculated and measured ^{1}H NMR chemical shifts for the hydrogens at the meso carbons suggests a ring current strength of about −22 nA/T under the experimental conditions, when assuming a linear relation between the ^{1}H NMR chemical shifts and the ring current strength.[55] The difference between the two values is most likely due to the use of the B3LYP functional that has problems to properly describe current densities for strongly antiaromatic porphyrinoids.[174]

Current density calculations show that for the neutral Zn(II)–octaethylporphyrin complex, the current pathway bifurcates into outer and inner routed at the pyrrolic rings as for other porphyrins, whereas for the Zn(II)–OEP dication and corresponding the neutral metal-free octaethylporphyrinoid, the ring current is sustained in the 16 π inner cross. Thus, no current passes the β carbons of the pyrrolic rings as illustrated in Fig. 9.

4.6 Ni(II)–norcorroles

The synthesis of Ni(II)–norcorrole has recently received attention since it is air and water stable and suitable as a cathode-active material for battery applications.[37] It is also considered to be the smallest antiaromatic porphyrinoid.[103] It has an order of magnitude higher electric conductivity than the corresponding aromatic Ni(II)–porphyrin complex, making the

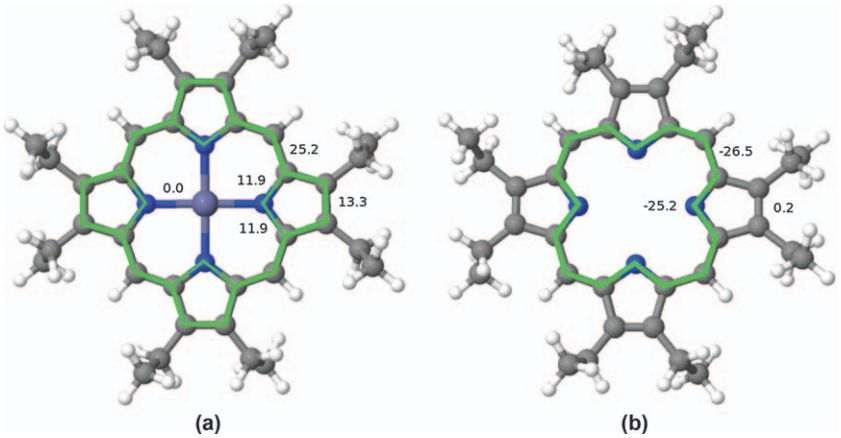

Fig. 9 Current strengths of (a) the neutral Zn(II)–octaethylporphyrin (Zn–OEP) complex and (b) the corresponding neutral metal-free octaethylporphyrinoid. The current pathway is indicated in green.

molecule attractive for future electronic devices.[38] It is also possible to introduce substituents such as a cyano group to antiaromatic Ni(II)–norcorroles *via* regioselective nucleophilic functionalization.[200]

Nozawa *et al.* reported recently the synthesis of an antiaromatic hydrogenated Ni(II)–tetrahydrocyanonorcorrole compound,[201] which is very interesting since antiaromatic hydrogenated porphyrinoids have not been previously synthesized. Hydrogenated porphyrins are common in natural and synthetic compounds such as chlorins and bacteriochlorins, whereas this does not hold for antiaromatic porphyrinoids. Nozawa *et al.*[201] combined experimental and theoretical methods such as ACID and NICS calculations for investigating the antiaromatic character of Ni(II)–cyanonorcorrole and its hydrogenated congener. ACID visualizations indicated a higher paratropic ring current for the hydrogenated compound as compared to the Ni(II)–cyanonorcorrole complex. The study suggested that for both molecules the main current density flow along the inner pathway. Thus, both molecules were assigned the same 16 π electron aromatic pathway. However, ^{1}H NMR measurements indicated that the pyrrolic protons of Ni(II)–tetrahydrocyanonorcorrole are shifted upfield relatively to those of nonaromatic porphyrinoids indicating a weakening of the antiaromatic character. The obtained experimental results contradict to some extent the picture deduced from ACID visualizations. The authors concluded that Ni(II)–cyanonorcorrole has a strong paratropic ring current, whereas for the hydrogenated molecule the paratropic ring current is weaker, even though the 16 π electron pathway remains after hydrogenation. Structural discrepancies between the two molecules were ruled out as a possible reason for their different behavior, because the HOMA indices were almost identical for the two molecules.

Cyclovoltametric measurements suggested that the hydrogenated molecule has a larger HOMO–LUMO gap, which might explain the weakening of the paratropic currents. It was concluded that in

Ni(II)–cyanonorcorrole diatropic currents circle in the pyrrolic rings that might enhance the paratropicity of the molecule. The authors considered it very challenging to provide an explanation for the difference in aromatic character of the two molecules leaving some important questions unanswered. The combination of ACID and NICS calculations was not enough to shed light on the problem described above. A current density study revealed that the two molecules have different current pathways.[202]

Ni(II)–cyanonorcorrole is strongly antiaromatic sustaining a paratropic ring current of −45.0 nA/T, whereas the hydrogenated molecule sustains a weaker paratropic ring current of −14.2 nA/T, which agrees with the interpretation by Nozawa *et al.*[201] Fig. 10a and c show the current flow and the integrated current strengths passing selected bonds of the two molecules, respectively. The current pattern is complicated showing that currents in the range of 2–4 nA/T pass the Ni(II) center. The current flow splits the pyrrolic rings with a stronger current of about −32 nA/T passing along the inner route. The current strength *via* the $C_\beta = C_\beta$ bond is about −13 nA/T. However, there is no strong local diatropic currents in the pyrrolic rings as suggested by Nozawa *et al.*[201] This example demonstrates the power of the integration analysis of current densities.

For Ni(II)–tetrahyrocyanonorcorrole the current also splits at the unsaturated pyrrolic rings. However, most of the current or about −11 nA/T passes the inner nitrogen, whereas only −1.8 nA/T takes the outer route. The hydrogenated pyrrolic rings sustain a weak local diatropic current of 2.3 nA/T, which might explain the observed ^{1}H NMR chemical shifts of the pyrrolic protons, whose chemical shifts are less upfield shifted than for nonaromatic porphyrinoids. The current flow and the integrated current strengths are shown in Fig. 10b and d.

4.7 Zn porphyrin arrays

Magnetically induced current density susceptibilities have been studied for several cyclic ethyne and butadiyne-bridged Zn(II)–porphyrin and isoporphyrin arrays.[203] Some of the studied porphyrin arrays are shown in Fig. 11, where the calculated current pathways are shown in pink and the integrated current strength susceptibility for selected bonds are given. Fig. 11a shows a metal-free isoporphyrin where the inner hydrogens have been moved to the meso carbons and saturating two of them. Isoporphyrin has a net current strength of 11.0 nA/T and is aromatic but weaker than free-base porphyrin that sustains a ring current of 27.0 nA/T. At the pyrrolic rings, the ring current is divided into an inner pathway of 8.5 nA/T and a weaker outer one of 3.0 nA/T.

The ethyne-bridged Zn(II)–porphyrin dimer is shown in Fig. 11b. The two Zn(II)–porphyrins are aromatic sustaining a ring current of 24.0 nA/T, whereas a weak paratropic current of 4.0 nA/T passes the ethyne bridge. The calculated ring current strength of Zn(II)–porphyrin is 26.6 nA/T.[203] Replacing the ethyne linker with a thiophene moiety does not change the picture. A paratropic current of 3.8 nA/T passes across the thiophene, which sustains a local diatropic ring current of 4.3 nA/T. The integrated current strengths passing selected bonds are shown in Fig. 11c.

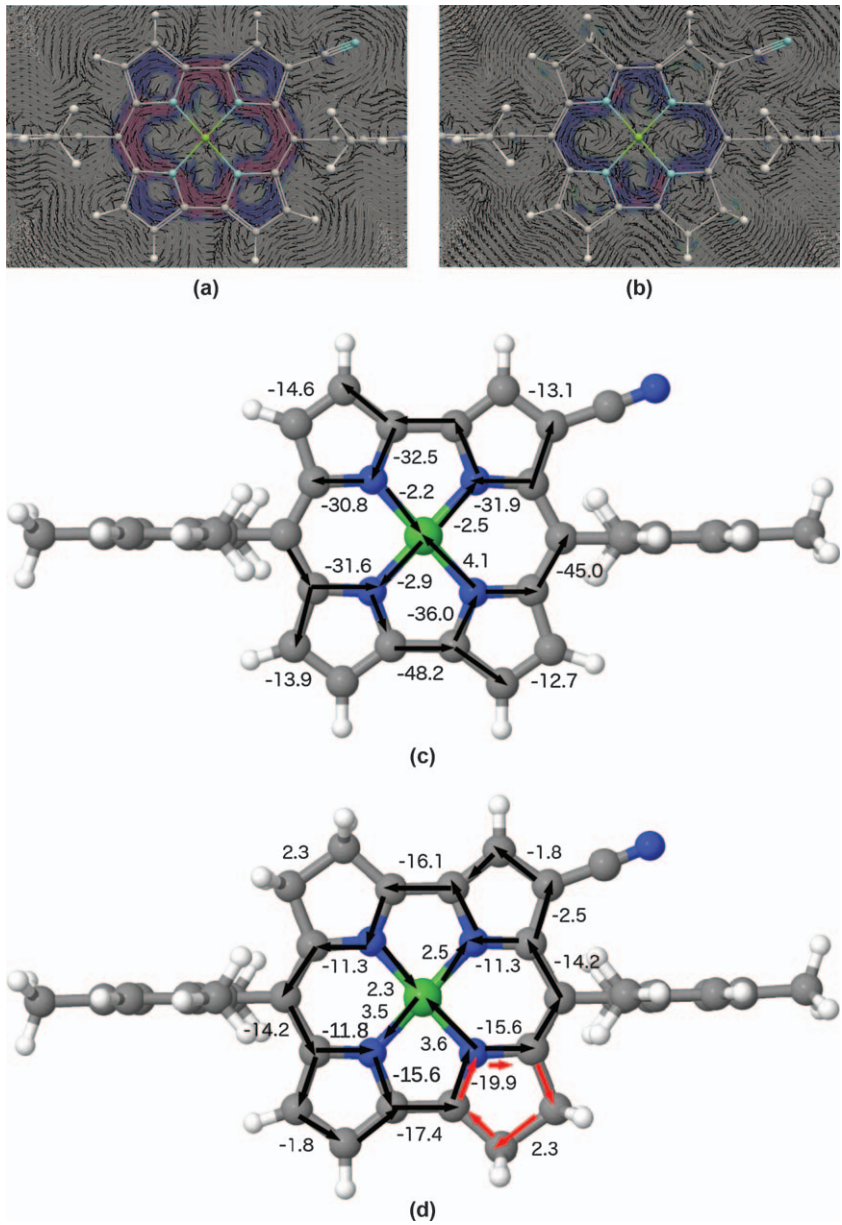

Fig. 10 The calculated current density in a plane 1 bohr above the molecule is shown using LIC streamlines for (a) Ni(II)–cyanonorcorrole and (b) Ni(II)–tetrahydrocyanonorcorrole. Stronger streamlines are visualized in pink and blue showing the preferred inner current pathway for both molecules. Integrated current strength susceptibilities for selected bonds are given for (c) Ni(II)–CN–norcorrole and (d) the hydrogenated Ni(II)–CN–norcorrole. The black and red arrows in (c) and (d) indicate direction of the current flow. Diatropic currents are assumed to circle clockwise.

Saturating the inner meso carbons leads to a significant change of the current flow as shown in Fig. 11d. A strong diatropic current of 21 nA/T passes across the ethyne bridge. The Zn(II)–porphyrinoid dimer is

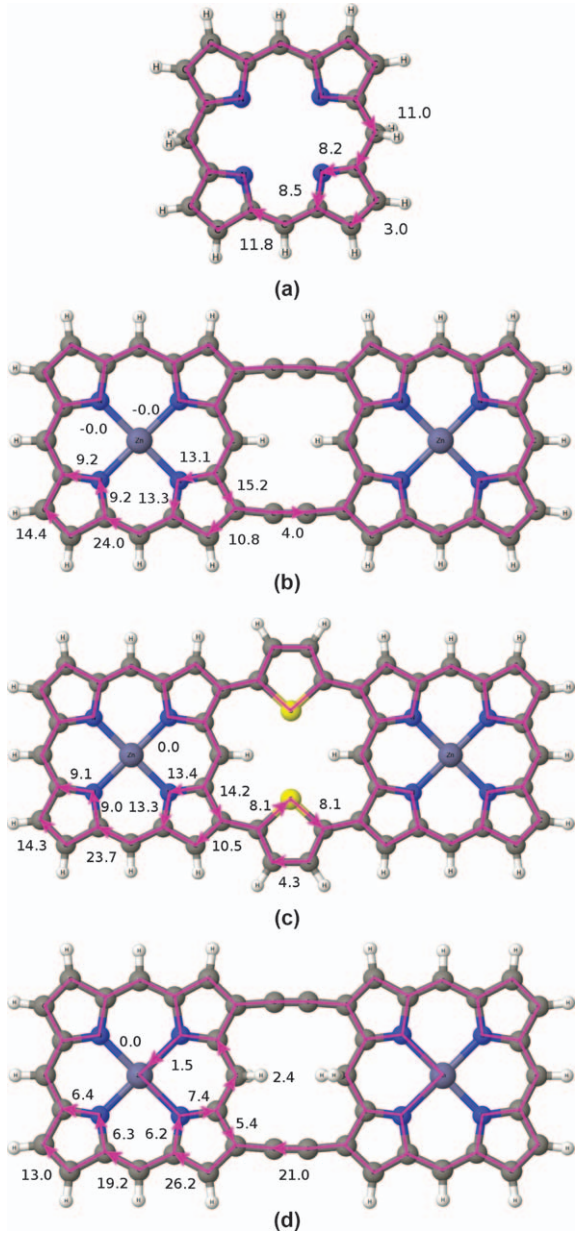

Fig. 11 Calculated current pathways and current strength susceptibilities (in nA/T) for (a) isoporphyrin with both inner hydrogens moved to the meso carbons, (b) ethyne-bridged Zn porphyrin dimer with saturated meso-carbon atoms in the inner ring, (c) thiophene-bridged porphyrin dimer and (d) neutral ethyne-bridged Zn porphyrin. Reproduced from ref. 203 with permission from The Royal Society of Chemistry. Diatropic currents are assumed to circle clockwise.

globally aromatic with local diatropic ring currents in the pyrrolic rings with the ethyne substitution, whereas the current splits into an inner and outer pathway at outer pyrrolic rings. Only a weak current of 2.4 nA/T passes the saturated meso carbons. Calculations on porphyrin trimers

and tetramers show that larger porphyrin arrays are locally aromatic, whereas almost no current passes the linkers between them.[203]

The aromatic character of the Zn(II)–porphyrin dimers can be understood by counting the number of π electrons. Each Zn(II)–porphyrin contributes with 26 π electrons and the two ethynes contribute with 4 π electrons yielding 56 π electrons, which corresponds to antiaromaticity. Thus, the individual porphyrins remain aromatic and a weak paratropic current passes between them. Replacing the ethyns with thiophenes does not alter the aromatic character because the thiophene bridged dimer has 64 π electrons. A globally aromatic dimer of Zn(II)–porphyrins with 54 π electrons is obtained when saturating two meso carbons.

4.8 Expanded and twisted porphyrins

The porphyrinoids discussed and presented so far were all planar or almost planar molecules implying that the well known Hückel π electron count rule can be applied. Thus, molecules with $(4n+2)$ π electrons are aromatic and those with $4n$ π electrons are antiaromatic. However, for molecules with a twisted structure with not all π orbitals oriented in the same direction, the aromaticity rules are different and more advanced methods to assess molecular aromaticity are needed. Molecules with Möbius-twisted topology have been synthesized. Singly Möbius twisted molecules have the π orbitals twisted by 180° along the conjugation pathway around the molecular macroring.[204,205] Assessing the aromatic character of twisted molecules is a challenge as shown by Taubert *et al.*[206] Heilbronner suggested that an inverted Hückel rule holds for singly twisted [4*n*]annulenes.[207] Thus, singly twisted Möbius type molecules with $4n$ π electrons are expected to be aromatic.

Molecules with more than one 180° twist, such as for example doubly twisted hexaphyrins,[208] do also belong to the class of molecules with Möbius topology. Synthesis of Möbius type porphyrinoids seems to be easier due to the conjugated pyrrole units than the synthesis of Möbius stabilized annulenes.[209–213] Möbius twisted expanded porphyrins have been synthesized and characterized.[214–226] The molecular aromaticity and magnetically induced current densities of the expanded and twisted porphyrins have also been studied computationally.[116,227–230]

In 2008, a more general π electron count rule was proposed for various types of twisted molecules. The generalized aromaticity rule is based on mathematical topology theory.[231] A Möbius twisted molecule is characterized by the linking number L_k, which is an integer that can be written as a sum of the twist (T_w) and the writhe (W_r), which are real numbers.[232–235] The T_w value is proportional to the overlap of the *p* orbitals around the ring. T_w is given by the sum of the local relative twists of the *p* orbitals with respect to the *p* orbitals of the adjacent atoms. The W_r value is a holistic property of the twisted ring that represents the curvature of the ring. For example, the twist of a ring can be released by allowing the ring to form multiple loops that increases the strain in the ring. T_w is transformed to W_r, whereas L_k is constant. The topological properties of Möbius twisted molecules have been described in detail by Rappaport

and Rzepa.[231] The aromatic character of twisted molecules is related to L_k as summarized in Table 3. Thus, molecules with an even L_k value are aromatic when they fulfill the $(4n+2)$ π-electron condition, while molecules with an odd L_k value are predicted to be aromatic when fulfilling the $4n$ π-electron count rule.[236] The linking number is considered to be the key quantity of the generalized π electron count rule.

The current density and current pathways have been studied for doubly Möbius-twisted meso-trifluoromethyl-substituted hexaphyrins, which were synthesized by Shimizu *et al.*,[208] which triggered a large number of experimental studies of twisted expanded porphyrins.[214,215,218,219,221,223,237–245] NICS calculations as well as atom in molecules (AIM) and electron localization function (ELF) critical point approaches have been used in studies of the aromatic properties of the doubly-twisted [26]hexaphyrin and [28]hexaphyrin molecules. Topological studies showed that the synthesized hexaphyrin molecules are formally doubly-twisted molecules with a linking number L_k of 2.[227,228,230,231,246] Thus, when applying the generalized Hückel aromaticity rule one expects that [26]hexaphyrin is aromatic and [28]hexaphyrin is antiaromatic. Experimental measurements of the ^{1}H NMR chemical shifts for the NH hydrogens showed indeed a downfield shift for [28]hexaphyrin as expected for the ^{1}H NMR chemical shifts of the hydrogens inside the paratropic current density flow of an antiaromatic molecule. However, the measured ^{1}H NMR signal for [26]hexaphyrin was also shifted by 11.11 ppm in the same direction, which was somewhat surprising, because the molecule should be aromatic according to the generalized π electron count rule.[208] Thus, from the experiment it was not clear whether [26]hexaphyrin should be considered aromatic or antiaromatic. Current densities and ^{1}H NMR chemical shifts were calculated in order to elucidate whether the synthesized hexaphyrins sustain diatropic or paratropic ring currents, that is, whether they are aromatic and antiaromatic molecules.[116]

Current density calculations on twisted molecular structures are much more challenging than on planar ones, because it is not obvious how to orient the external magnetic field relative to the molecular frame. The ring-current strengths were therefore calculated for different magnetic field directions. Fig. 12 shows how different directions of the external field affect the ring-current strength susceptibility. The ring-current strength susceptibilities calculated as a function of the angle of the external magnetic field with respect to the molecule frame have a maximum or minimum depending on whether the studied molecule is aromatic or antiaromatic. The calculations showed that [26]hexaphyrin is indeed aromatic according to the ring current criterion. The calculated

Table 3 The generalized π-electron count rules where the aromatic character is given by the linking number L_k.[231]

L_k	$(4n+2)$ π	$4n$ π
0	Aromatic	Antiaromatic
Even	Aromatic	Antiaromatic
Odd	Antiaromatic	Aromatic

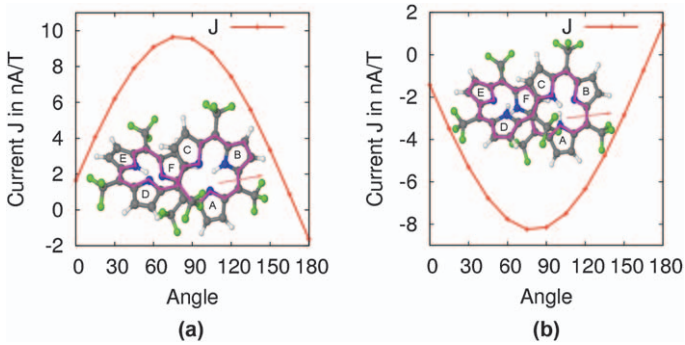

Fig. 12 Calculated ring-current strength susceptibilities for doubly twisted hexaphyrins. The current strength passing the bond indicated with the red arrow was calculated using different orientations of the external magnetic field. Angles are given in degrees. The dominating current pathway is indicated in pink. (a) The aromatic [26]hexaphyrin has a maximum ring-current strength susceptibility of 9.6 nA/T. (b) The antiaromatic [28]hexaphyrin has a minimum ring-current strength susceptibility of −8.2 nA/T.[116]

^{1}H NMR chemical shifts also agreed with the measured ones, suggesting that N-H$\cdots$F interactions are responsible for the observed anomalous ^{1}H NMR chemical shift.

Calculations on [24]hexaphyrin, [26]hexaphyrin, [28]hexaphyrin, and [30]hexaphyrin yielded alternation direction of the ring-current flow for these molecules. The generalized Hückel rule for $L_k = 2$ is fulfilled; molecules with $4n + 2$ π electrons are aromatic and $4n$ π electrons lead to antiaromaticity. Thus, it is remarkable that the aromaticity rule derived for planar molecules and generalized to twisted molecules also holds for the strongly deformed hexaphyrins.[116] The current density calculations show that all π electrons participate in the current density flow around the hexaphyrin ring. It might be as correct to assign 36π–42π electrons to the aromatic ring of the [24]hexaphyrin-[30]hexaphyrin molecules, respectively, as discussing their 24π–30π electron pathways. The current density flow splits at many of the pyrrolic rings taking both the outer and the inner route as for free-base porphyrin.

An even greater challenge was to synthesize singly Möbius twisted molecules. Herges *et al.* managed to synthesize the first singly Möbius twisted molecule, which was a [16]annulene.[205,247,248] They synthesized also the corresponding untwisted [16]annulene. However, current density calculations and NICS calculations showed that the Möbius twisted and the untwisted Hückel [16]annulenes were nonaromatic.[206,249]

The phosphorousoxide (PO) bridged [28]hexaphyrin and $(PO)_2$ bridged [30]hexaphyrin shown in Fig. 13 are the first aromatic and antiaromatic singly Möbius twisted molecules that have been synthesized.[224] Current density calculations showed that the PO bridged [28]hexaphyrin is aromatic and the $(PO)_2$ bridged [30]hexaphyrin is antiaromatic fulfilling the generalized Hückel rule for singly Möbius twisted molecular rings.[229] The maximum current strength calculated for PO-[28]hexaphyrin is 14.9 nA/T, whereas $(PO)_2$-[30]hexaphyrin sustains a maximum paratropic ring current of −10.3 nA/T. The ring current splits into an inner and outer pathway at most of the pyrrolic rings.

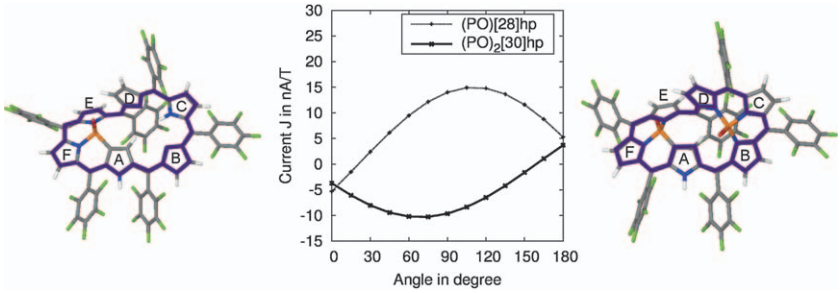

Fig. 13 Calculated ring-current strength susceptibilities for singly twisted hexaphyrins. The ring-current strength susceptibility was calculated using different orientations of the external magnetic field. Angles are given in degrees. The dominating current pathway is indicated in in violet. (left) The aromatic PO bridged [28]hexaphyrin has a maximum current strength susceptibility of 14.9 nA/T. (right) The antiaromatic $(PO)_2$ bridged [30]hexaphyrin has a minimum current strength susceptibility of –10.3 nA/T.[229]

4.9 Contracted porphyrins

Contracted porphyrins or subporphyrins are porphyrinoids with less than four pyrrolic rings.[250–253] For example, by starting from the corrole structure and removing one pyrrole ring leads to a subporphyrin consisting of three pyrrolic rings connected *via* methin bridges. Subporphyrins are thought to have a 14 π-electron aromatic pathway as compared to the 18 π-electron pathway for porphyrins.

Subporphyrins have the typically C_3 symmetric bowl shaped structures with a boron center as shown in Fig. 14. They exhibit interesting nonlinear optical properties due to the octupolar structure.[34,252] Tripyrin has a similar structure but without the boron center. It has a richer coordination chemistry as compared to subporphyrin. Tripyrin and subporphyrins are useful building blocks in supramolecular architectures.[34,35,252] Very few computational studies on contracted porphyrins have been published.[50,254–256] Current density calculations have been performed on [14]tribenzosubporphine(1.1.1)hydroxyboron(III) and [14]subporphine(1.1.1)hydroxyboron(III) complexes using the CTOCD-DZ approach.[256] The calculations showed that the current density flow does not follow the expected 14 π-electron pathway.[256] It flows instead mainly along the inner edge of the macroring suggesting that further current density studies on contracted porphyrins might be of interest.

4.10 Optical and magnetic properties of antiaromatic porphyrinoids

Magnetizabilities and magnetically induced ring-current strength susceptibilities have been studied for closed-shell porphyrinoids with aromatic properties ranging from nonaromatic to antiaromatic. The calculations showed that there is a linear relation between magnetizabilities and ring-current strength susceptibilities as shown in Fig. 15.[174]

The linear relation is not surprising when realizing that the magnetizability can be obtained by integrating the current density susceptibility tensor multiplied with the vector potential of the external magnetic field as in eqn (8). The calculations showed that the porphyrinoids with the largest paratropic ring-current strength susceptibility are closed-shell

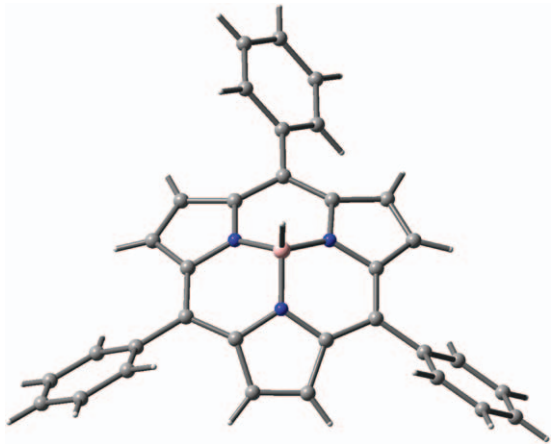

Fig. 14 A subporphyrin with boron at the center and phenyl substituents in the meso positions. The structure has been reported in ref. 253.

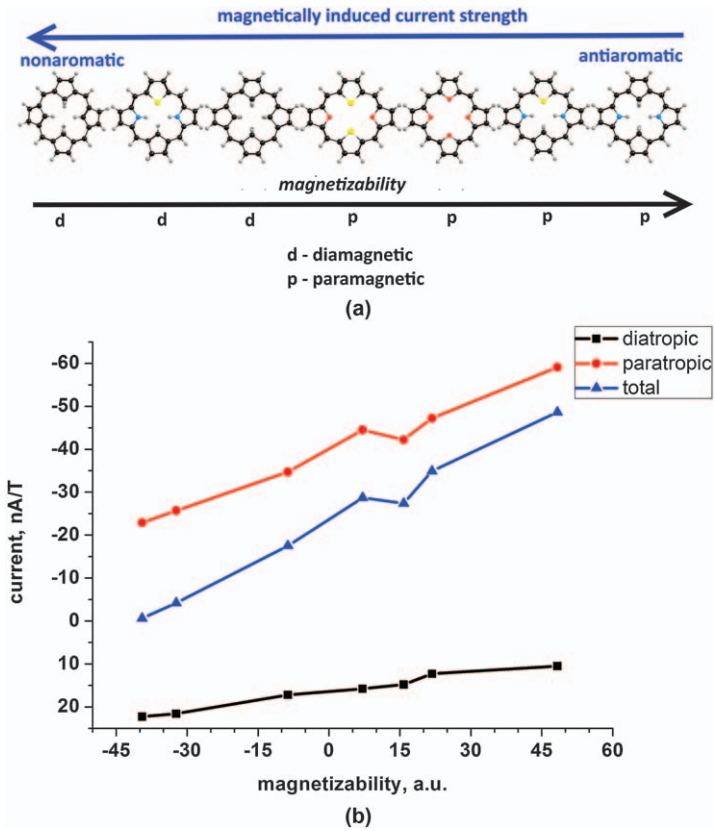

Fig. 15 (a) The relation between the calculated magnetically induced ring-current strength susceptibilities and magnetizabilities of antiaromatic porphyrinoids, where d and p stand for diamagnetic and paramagnetic, respectively. (b) The magnetizabilities of the porphyrinoids calculated at the MP2 level showing the transition from diamagnetism to paramagnetism with increasing strength of the paratropic ring current. Reproduced from ref. 174 with permission from The Royal Society of Chemistry.

paramagnetic molecules with positive magnetizabilities. Paramagnetism is usually associated with the non-zero electronic spin of open-shell electronic configurations,[257] whereas closed-shell paramagnetic molecules are rare.[258] However, eqn (9) shows that large paratropic ring currents might also lead to paramagnetism due to contributions from the angular momentum operator.[174,259–261]

Computational studies of the lowest excited states of antiaromatic porphyrinoids show that the excitation energy of the first excited state decreases with increasing ring-current strength susceptibility, whereas the excitation energy of higher-lying excited states are almost independent of the ring-current strength susceptibility.[262] They also show that the paratropic contribution to the magnetically induced ring-current strength susceptibility and the magnetic dipole-transition moment between the ground and the lowest excited state are related as shown in Fig. 15. The large magnetic transition moment of the $S_0 \rightarrow S_1$ excitation is the main contribution to the magnetically induced ring-current strength susceptibility of the antiaromatic porphyrinoids. The small excitation energy of the magnetically allowed $S_0 \rightarrow S_1$ transition leads to the very large paratropic ring-current susceptibilities and paramagnetism (Fig. 16).

4.11 Circulenes

Circulenes are not porphyrinoids but consist of fully annelated phenylenes which leads to circular planar or almost planar structures that have very complicated current pathways, which are difficult to predict without performing current density calculations. When the bridging units that connect phenylenes at the outer edge are NH moieties as in tetraaza[8]circulene, the molecule consists of alternating annelated inverted pyrrolic rings and phenyl rings forming a macro ring. Circulenes can also be considered consisting of an inner macroring called the hub and an outer macroring called the rim. The hub and the rim are connected *via* the common bonds of the annelated rings, see Fig. 17a.

For [8]circulenes, the hub consist of an inner eight-membered cyclooctatetraene (COT) ring with 8 π electrons. For symmetry reasons, the number of π electrons along the rim is $4n$. Thus, neutral [8]circulenes fulfill Hückel's rule for antiaromaticity, when the same kind of bridging unit connects the phenylene rings along the rim. The aromatic character and current pathways of [8]circulenes with different bridging units have been calculated.[266–268]

Replacing the connecting rim moiety X in Fig. 17a with formally isoelectronic heteroatoms or molecular moieties such as C=O, S, Se, P = H, As-H, or CH_2 does not lead to a substantial change of the aromaticity.[266–268] Instead the system remains nonaromatic or weakly antiaromatic. Insertion of larger heteroatoms or molecular moieties containing larger heteroatoms might lead to structural distortions of the [8]circulene.

In neutral [8]circulene, the hub sustains a paratropic current, whereas the rim carries a diatropic current contribution of the same size but in the opposite direction. The net ring current vanishes leading to a

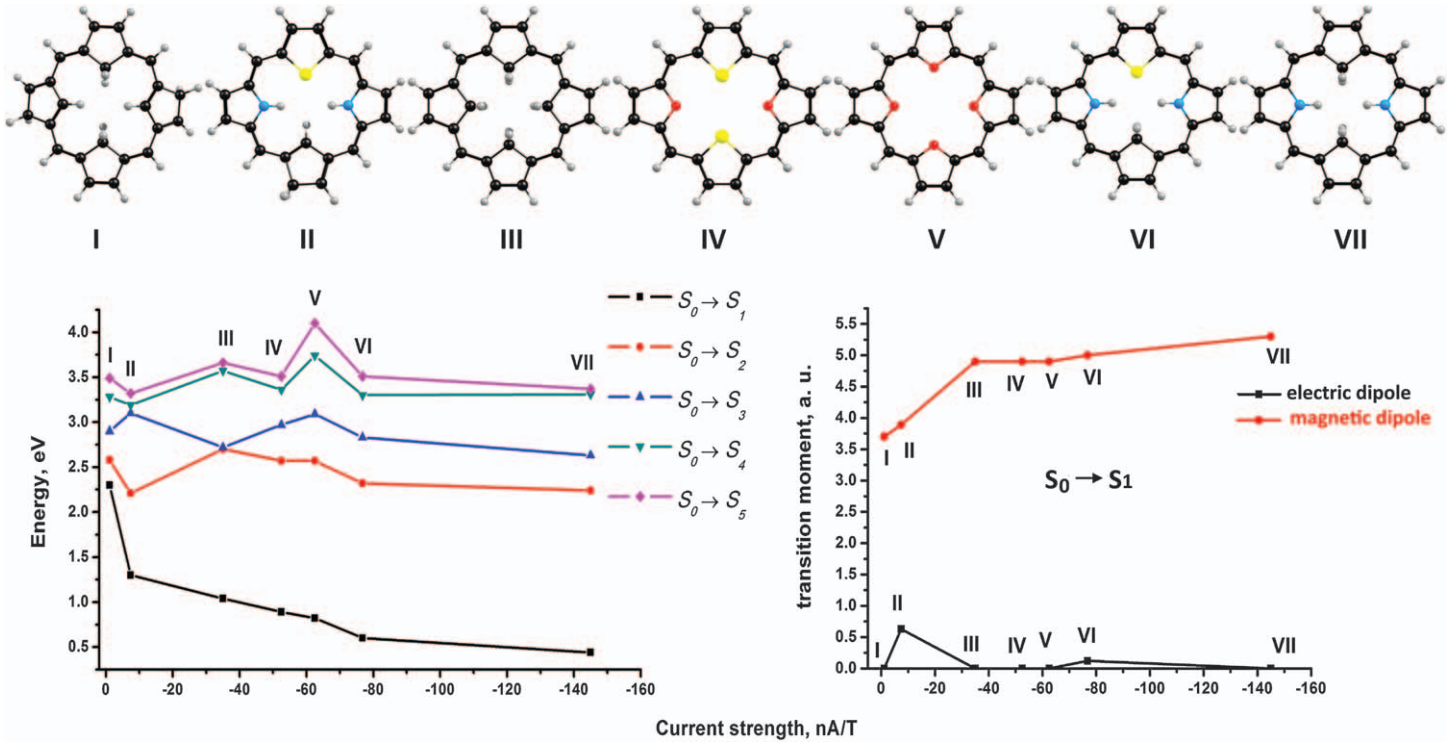

Fig. 16 The lowest vertical transition energies as well as the electric and magnetic transition dipole moments of antiaromatic porphyrinoids calculated at the approximate second-order coupled-cluster (CC2) level.[263–265] Reproduced from ref. 262 with permission from The Royal Society of Chemistry.

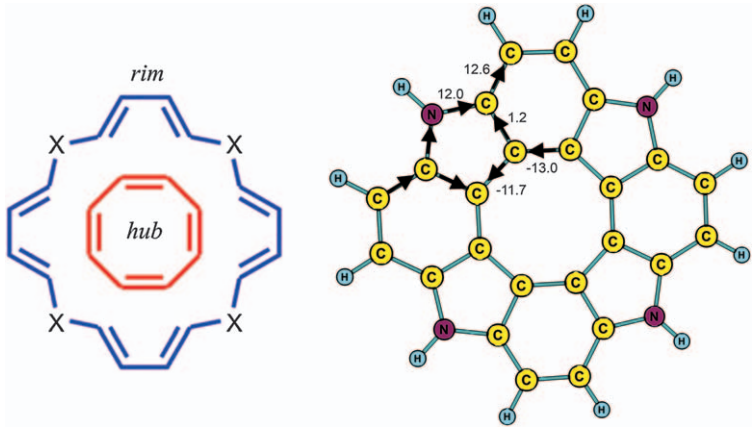

Fig. 17 (a) The inner hub and the outer rim of [8]circulenes are shown. (b) The current pathways in tetra-aza[8]circulene.[266–268]

nonaromatic character. The aromatic character can be changed by adding or removing two electrons, because the doubly charged [8]circulenes fulfill Hückel's rule for aromaticity.[266–268] The aromatic character follows the Hückel rule for disc-shaped molecules. However, the strength of the current flow is difficult to estimate without performing explicit current density calculations.

5 Outlook

Current density calculations can be a very useful complement to experimental studies, since the obtained current densities provide information about the electronic structure that is difficult to determine experimentally. Molecular aromaticity is a frequently used concept in chemistry. However, it does not have any unique and well-defined definition. One of the experimental means to determine the degree of aromaticity is to scrutinize measured ^{1}H NMR chemical shifts, which depend on the pathways of the magnetically induced current density and ring-current strengths. Aromatic properties and the degree of aromaticity of complex molecular structures can be estimated by performing calculations of magnetically induced current densities accompanied with a detailed integration analysis of the current flow along selected chemical bonds. Such analyses can be performed on general molecules with nonplanar and even twisted molecular rings.

Knowledge about magnetically induced current densities is also useful in other contexts, because magnetically induced current densities are as fundamental as electron densities when studying molecular magnetic properties and their relations to molecular optical properties. Recent studies on antiaromatic porphyrinoids indicate that antiaromaticity is closely related to strong magnetic transitions in electronic spectra. A future direction of current density calculations is towards studies of larger nanosized molecules with large current density susceptibilities. Such studies requires computational methods that are aimed for

calculations on very large molecules. We are presently developing novel computational approaches for tackling large molecules.[269]

Acknowledgements

H.F. thanks the Norwegian Research Council through the CoE Centre for Theoretical and Computational Chemistry (Grant No. 179568/V30 and 231571/F20) for support. This work has received support from the Norwegian Supercomputing Program (NOTUR) through a grant of computer time (Grant No. NN4654K). It was also supported by The Academy of Finland through projects 275845 and 297304 and by the Magnus Ehrnrooth Foundation. The authors acknowledge CSC – IT Center for Science, Finland and the Finnish Grid and Cloud Infrastructure (FGCI) for computational resources. F.P. thanks the Graduate School of Engineering of Tohoku University for financial support.

References

1 C. Wang, H. Dong, W. Hu, Y. Liu and D. Zhu, *Chem. Rev.*, 2012, **112**, 2208–2267.
2 M. Jurow, A. E. Schuckman, J. D. Batteas and C. M. Drain, *Coord. Chem. Rev.*, 2010, **254**, 2297–2310.
3 T. Tanaka and A. Osuka, *Chem. Soc. Rev.*, 2015, **44**, 943–969.
4 J. Chou, M. E. Kosal, H. S. Nalwa, N. A. Rakow and K. S. Suslick, *Porphyrin Handbook*, Academic Press, San Diego, CA, 2000, vol. 6, pp. 41–128.
5 L.-L. Lia and E. Wei-Guang Diau, *Chem. Soc. Rev.*, 2013, **42**, 291–304.
6 R. Mera-Adasme, W.-H. Xu, D. Sundholm and F. Mendizabal, *Phys. Chem. Chem. Phys.*, 2016, **18**, 27877–27884.
7 R. Paolesse, S. Nardis, D. Monti, M. Stefanelli and C. Di Natale, *Chem. Rev.*, 2017, **117**, 2517–2583.
8 G. de la Torre, G. Bottari, M. Sekita, A. Hausmann, D. M. Guldi and T. Torres, *Chem. Soc. Rev.*, 2013, **42**, 8049–8105.
9 R. K. Pandey and G. Zheng, *Porphyrin Handbook*, Academic Press, San Diego, CA, 2000, vol. 6, pp. 157–230.
10 J. R. H. Huang, W. Song and J. F. Lovell, *Front. Phys.*, 2015, **3**, 23–1–15.
11 J. L. Sessler, S. J. Weghorn, Y. Hiseada and V. Lynch, *Chem. – Eur. J.*, 1995, **1**, 56–67.
12 J. L. Sessler, S. J. Weghorn, Y. Hiseada and V. Lynch, *J. Am. Chem. Soc.*, 1990, **112**, 2810–2813.
13 A. Berlicka, P. Dutka, L. Szterenberg and L. Latos-Grażyński, *Angew. Chem., Int. Ed.*, 2014, **53**, 4885–4889.
14 S. Aronoff and M. Calvin, *J. Org. Chem.*, 1943, **8**, 205–223.
15 M. O. Senge, *Angew. Chem., Int. Ed.*, 2011, **50**, 4272–4277.
16 K. Berlin, *Angew. Chem., Int. Ed.*, 1996, **35**, 1820–1822.
17 T. D. Lash and S. T. Chaney, *Chem. – Eur. J.*, 1996, **2**, 944–948.
18 M. Pawlicki and L. Latos-Grażyński, *Chem. Rec.*, 2006, **6**, 64–78.
19 *The Porphyrins*, ed. D. Dolphin, Academic Press, London and New York, 1978.
20 D. Sundholm, H. Konschin and M. Häser, *Chem. – Eur. J.*, 1999, **5**, 267–273.
21 J. Helaja, F. P. Montfors, I. Kilpeläinen and P. H. Hynninen, *J. Org. Chem.*, 1999, **64**, 432–437.

22 E. Hückel, *Grundzüge der Theorie ungesättigter und aromatischer Verbindungen*, Verlag Chemie, Berlin, 1938.
23 W. von Eggers, Doering and F. L. Detert, *J. Am. Chem. Soc.*, 1951, **73**, 876–877.
24 M. Solá, *Front. Chem.*, 2017, **5**, 22.
25 R. Hoffmann, *Am. Sci.*, 2015, **103**, 18–22.
26 S. K. Ritter, *Chem. Eng. News*, 2015, **93**, 37–38.
27 J. I. Wu, I. Fernandez and P. v. R. Schleyer, *J. Am. Chem. Soc.*, 2013, **135**, 315–321.
28 H. Fliegl and D. Sundholm, *J. Org. Chem.*, 2012, **77**, 3408–3414.
29 R. R. Valiev and V. N. Cherepanov, *Int. J. Quantum Chem.*, 2013, **113**, 2563–2567.
30 S. Hiroto, Y. Miyake and H. Shinokubo, *Chem. Rev.*, 2017, **117**, 2910–3043.
31 S. Saito and A. Osuka, *Angew. Chem., Int. Ed.*, 2011, **50**, 4342–4373.
32 J.-Y. Shin, K. S. Kim, M.-C. Yoon, J. M. Lim, Z. S. Yoon, A. Osuka and D. Kim, *Chem. Rev.*, 2010, **39**, 2751–2767.
33 T. Tanaka and A. Osuka, *Chem. Rev.*, 2017, **117**, 2584–2640.
34 S. Shimizu, *Chem. Rev.*, 2017, **117**, 2730–2784.
35 C. G. Claessens, D. González-Rodríguez, M. S. Rodríguez-Morgade, A. Medina and T. Torres, *Chem. Rev.*, 2014, **114**, 2192–2277.
36 A. Ghosh, *Chem. Rev.*, 2017, **117**, 3798–3881.
37 J-Y. Shin, T. Yamada, H. Yoshikawa, K. Awaga and H. Shinokubo, *Angew. Chem., Int. Ed.*, 2014, **53**, 3096–3101.
38 S. Fujii, S. Marqués-González, J. Shin, H. Shinokubo, T. Masuda, T. Nishino, N. P. Arasu, H. Vázquez and M. Kiguchi, *Nat. Commun.*, 2017, **8**, 15984-1–8.
39 T. D. Lash, *Chem. Rev.*, 2017, **117**, 2313–2446.
40 T. D. Lash, *Eur. J. Org. Chem.*, 2007, **135**, 5461–5481.
41 R. R. Valiev, H. Fliegl and D. Sundholm, *J. Phys. Chem. A*, 2015, **119**, 1201–1207.
42 R. R. Valiev, H. Fliegl and D. Sundholm, *Phys. Chem. Chem. Phys.*, 2015, **17**, 14215–14222.
43 I. Benkyi, H. Fliegl, R. R. Valiev and D. Sundholm, *Phys. Chem. Chem. Phys.*, 2016, **18**, 11932–11941.
44 R. B. Woodward, *Angew. Chem.*, 1960, **72**, 651–662.
45 J. S. Reddy and V. G. Anand, *J. Am. Chem. Soc.*, 2008, **130**, 3718–3719.
46 B. K. Reddy, A. Basavarajappa, M. D. Ambhore and V. G. Anand, *Chem. Rev.*, 2017, **117**, 3420–3443.
47 B. K. Reddy, J. Rawson, S. C. Gadekar, P. Kogerler and V. G. Anand, *Chem. Commun.*, 2017, **53**, 8211–8214.
48 T. Chatterjee, V. S. Shetti, R. Sharma and M. Ravikanth, *Chem. Rev.*, 2017, **117**, 3254–3328.
49 J. Waluk, *Chem. Rev.*, 2017, **117**, 2447–2480.
50 J. Mack, *Chem. Rev.*, 2017, **117**, 3444–3478.
51 D. Sundholm, H. Fliegl and R. J. Berger, *WIREs Comput. Mol. Sci.*, 2016, **6**, 639–678.
52 J. M. Sung, J. Oh, W.-Y. Cha, W. Kim, J. M. Lim, M.-C. Yoon and D. Kim, *Chem. Rev.*, 2017, **117**, 2257–2312.
53 R. R. Valiev, H. Fliegl and D. Sundholm, *J. Phys. Chem. A*, 2013, **117**, 9062–9068.
54 R. R. Valiev, H. Fliegl and D. Sundholm, *Phys. Chem. Chem. Phys.*, 2014, **16**, 11010–11016.
55 H. Fliegl, F. Pichierri and D. Sundholm, *J. Phys. Chem. A*, 2015, **119**, 2344–2350.

56 R. Gershoni-Poranne and A. Stanger, *Chem. Soc. Rev.*, 2015, **44**, 6597–6615.
57 P. von Ragué Schleyer and H. Jiao, *Pure Appl. Chem.*, 1996, **28**, 209–218.
58 A. Stanger, *Chem. Commun.*, 2009, 1939–1947.
59 K. Jug and A. Köster, *J. Phys. Org. Chem.*, 1991, **4**, 163–169.
60 J. Neus, *Aromatizität: Geschichte und mathematische Analyse eines fundamentalen chemischen Begriffs*, HYLE Publications, Karlsruhe, 2002.
61 C. W. Bird, *Tetrahedron*, 1996, **52**, 9945–9952.
62 P. W. Fowler, E. Steiner, R. W. A. Havenith and L. W. Jenneskens, *Magn. Reson. Chem.*, 2004, **42**, S68–S78.
63 J. Aihara, *J. Am. Chem. Soc.*, 2006, **128**, 2873–2879.
64 M. K. Cyrañski, T. M. Krygowski, A. R. Katritzky and P. von Ragué Schleyer, *J. Org. Chem.*, 2002, **67**, 1333–1338.
65 A. R. Katritzky, P. Barczyński, G. Musumarra, D. Pisano and M. Szafran, *J. Am. Chem. Soc.*, 1989, **111**, 7–15.
66 F. Feixas, E. Matito, J. Poater and M. Solá, *J. Comput. Chem.*, 2008, **29**, 1543–1554.
67 T. M. Krygowski and M. K. Cyrański, *Chem. Rev.*, 2001, **101**, 1385–1420.
68 B. Kovacević, D. Barić, Z. B. Maksić and T. Müller, *ChemPhysChem*, 2004, **5**, 1352–1364.
69 H. Fallah-Bagher-Shaidaei, C. S. Wannere, C. Corminboeuf, R. Puchta and P. von Ragué Schleyer, *Org. Lett.*, 2006, **8**, 863–866.
70 H. M. Goff, *Bioinorg. Chem.*, 1978, **9**, 61–79.
71 M. Gouterman, *J. Mol. Spectrosc.*, 1961, **6**, 138–163.
72 M. Gouterman, *The Porphyrins Vol. III*, Academic Press, London and New York, 1978, p. 1.
73 N. Kobayashi and K. Nakaia, *Chem. Commun.*, 2007, 4077–4092.
74 J. Mack, M. J. Stillman and N. Kobayashi, *Coord. Chem. Rev.*, 2007, **251**, 429–453.
75 J. Sebek and P. Bour, *J. Phys. Chem. A*, 2008, **112**, 2920–2929.
76 H. Lu and N. Kobayashi, *Chem. Rev.*, 2016, **116**, 6184–6261.
77 J. P. Macquet, M. M. Millard and T. Theophanides, *J. Am. Chem. Soc.*, 1978, **100**, 4741–4746.
78 H. Lee, S.-Y. An and C. Minhaeng, *J. Phys. Chem. B*, 1999, **103**, 4992–4996.
79 T. V. Esipova, H. J. Rivera-Jacquez, B. Weber, A. E. Masunov and S. A. Vinogradov, *J. Am. Chem. Soc.*, 2016, **138**, 15648–15662.
80 Y. Fang, Z. Ou and K. M. Kadish, *Chem. Rev.*, 2016, **117**, 3377–3419.
81 F. D'Souza, *J. Porphyrins Phthalocyanines*, 2002, **6**, 285–288.
82 U. Fleischer, W. Kutzelnigg, P. Lazzeretti and V. Muehlenkamp, *J. Am. Chem. Soc.*, 1994, **116**, 5298–5306.
83 J. A. Pople and K. G. Untch, *J. Am. Chem. Soc.*, 1966, **88**, 4811–4815.
84 H. M. McConnell, *J. Chem. Phys.*, 1957, **27**, 226–229.
85 J. Jusélius, M. Patzschke and D. Sundholm, *J. Mol. Struct.: THEOCHEM*, 2003, **633**, 123–136.
86 C. S. Wannere and P. von Ragué Schleyer, *Org. Lett.*, 2003, **5**, 605–608.
87 J. Pople, *Mol. Phys.*, 1958, **1**, 175–180.
88 R. McWeeny, *Mol. Phys.*, 1958, **1**, 311–321.
89 J. A. N. F. Gomes and R. B. Mallion, *Chem. Rev.*, 2001, **101**, 1349–1384.
90 P. Lazzeretti, *Prog. Nucl. Magn. Reson. Spectrosc.*, 2000, **36**, 1–88.
91 K. K. Baldridge and M. S. Gordon, *J. Am. Chem. Soc.*, 1988, **110**, 4204–4208.
92 L. Nyulaszi, T. Karpati and T. Veszpremi, *J. Am. Chem. Soc.*, 1994, **116**, 7239–7242.
93 M. N. Glukhovtsev, R. D. Bach and S. Laiter, *J. Mol. Struct.: THEOCHEM*, 1997, **417**, 123–129.

94 D. Sundholm, R. J. F. Berger and H. Fliegl, *Phys. Chem. Chem. Phys.*, 2016, **18**, 15934–15942.
95 J. Cao, G. London, O. Dumele, M. von Wantoch Rekowski, N. Trapp, L. Ruhlmann, C. Boudon, A. Stanger and F. Diederich, *J. Am. Chem. Soc.*, 2015, **137**, 7178–7188.
96 G. C. J. G. Hernández-Lima, J. E. Barquera-Lozada and F. Cortés-Guzmán, *J. Comput. Chem.*, 2015, **36**, 1573–1578.
97 K. Abersfelder, A. J. P. White, R. J. F. Berger, H. S. Rzepa and D. Scheschkewitz, *Angew. Chem., Int. Ed.*, 2011, **50**, 7936–7939.
98 C. Stassis, *Phys. Rev. Lett.*, 1970, **24**, 1415–1416.
99 C. Wilkinson, D. A. Keen, P. J. Brown and J. B. Forsyth, *J. Phys.: Condens. Matter*, 1989, **1**, 3833–3839.
100 D. Sundholm, *Phys. Chem. Chem. Phys.*, 2000, **2**, 2275–2281.
101 F. Santoro, A. Lami, R. Improta, J. Bloino and V. Barone, *J. Chem. Phys.*, 2008, **128**, 224311.
102 S. Mori and A. Osuka, *J. Am. Chem. Soc.*, 2005, **127**, 8030–8031.
103 T. Ito, Y. Hayashi, S. Shimizu, J. Shin, N. Kobayashi and H. Shinokubo, *Angew. Chem., Int. Ed.*, 2012, **51**, 8542–8545.
104 N. Kobayashi and K. Nakai, *Chem. Commun.*, 2007, 4077–4092.
105 J. Mack and N. Kobayashi, *Chem. Rev.*, 2011, **111**, 281–321.
106 J. Michl, *J. Am. Chem. Soc.*, 1978, **100**, 6801–6811.
107 J. Michl, *Tetrahedron*, 1984, **40**, 3845–3934.
108 U. Höweler, J. W. Downing, J. Fleischhauer and J. Michl, *J. Chem. Soc., Perkin Trans.*, 1998, **2**, 1101–1117.
109 J. Fleischhauer, U. Höweler and J. Michl, *Spectrochim. Acta, Part A*, 1999, **55**, 585–606.
110 J. Fleischhauer, U. Höweler and J. Michl, *J. Phys. Chem. A*, 2000, **104**, 7762–7775.
111 T. Hoshi and N. Kobayashi, *Coord. Chem. Rev.*, 2017, **345**, 31–41.
112 J. M. Lim, Z. S. Yoon, J. Shin, K. S. Kim, M. Yoon and D. Kim, *Chem. Commun.*, 2009, 261–273.
113 S. Cho, Z. S. Yoon, K. S. Kim, M. Yoon, D. Cho, J. L. Sessler and D. Kim, *J. Phys. Chem. Lett.*, 2010, **1**, 895–900.
114 T. M. Krygowski, *Chem. Inf. Comput. Sci.*, 1993, **33**, 70–78.
115 M. K. Cyrañski, T. M. Krygowski, M. Wisiorowski, N. J. R. van Eikema, Hommes and P. von Ragué Schleyer, *Angew. Chem., Int. Ed.*, 1998, **37**, 177–180.
116 H. Fliegl, D. Sundholm, S. Taubert and F. Pichierri, *J. Phys. Chem. A*, 2010, **114**, 7153–7161.
117 T. M. Krygowski, M. K. Cyrañski, Z. Czarnocki, G. Häfelinger and A. R. Katritzky, *Tetrahedron*, 2017, **56**, 1783–1796.
118 R. Herges and D. Geuenich, *J. Phys. Chem. A*, 2001, **105**, 3214–3220.
119 D. Geuenich, K. Hess, F. Köhler and R. Herges, *Chem. Rev.*, 2005, **105**, 3758–3772.
120 H. Fliegl, J. Jusélius and D. Sundholm, *J. Phys. Chem. A*, 2016, **120**, 5658–5664.
121 P. von Ragué Schleyer, C. Maerker, A. Dransfeld, H. Jiao and N. J. R. van Eikema Hommes, *J. Am. Chem. Soc.*, 1996, **118**, 6317–6318.
122 S. Van Damme, G. Acke, R. W. A. Havenith and P. Bultinck, *Phys. Chem. Chem. Phys.*, 2016, **18**, 11746–11755.
123 I. Morao, B. Lecea and F. P. Cossío, *J. Org. Chem.*, 1997, **62**, 7033–7036.
124 M. Bühl, *Chem. – Eur. J.*, 1998, **4**, 734–739.
125 J. Jusélius and D. Sundholm, *Phys. Chem. Chem. Phys.*, 1999, **1**, 3429–3435.

126 J. Jusélius and D. Sundholm, *Phys. Chem. Chem. Phys.*, 2000, **2**, 2145–2151.
127 S. Klod and E. Kleinpeter, *J. Chem. Soc. Perkin Trans.* **2**, 2001, 1893–1898.
128 S. Klod, A. Koch and E. Kleinpeter, *J. Chem. Soc. Perkin Trans.* **2**, 2002, 1506–1509.
129 A. Muñoz-Castro, *Chem. Phys. Lett.*, 2011, **517**, 113–115.
130 P. Lazzeretti, *Phys. Chem. Chem. Phys.*, 2004, **6**, 217–223.
131 S. Pelloni, G. Monaco, P. Lazzeretti and R. Zanasi, *Phys. Chem. Chem. Phys.*, 2011, **13**, 20666–20672.
132 J. O. C. Jiménez-Halla, E. Matito, J. Robles and M. Solá, *J. Organomet. Chem.*, 2006, **691**, 4359–4366.
133 S. Pelloni and P. Lazzeretti, *J. Phys. Chem. A*, 2013, **117**, 9083–9092.
134 Z. Badri, S. Pathak, H. Fliegl, P. Rashidi-Ranjbar, R. Bast, R. Marek, C. Foroutan-Nejad and K. Ruud, *J. Chem. Theory Comput.*, 2013, **9**, 4789–4796.
135 G. Monaco and R. Zanasi, *J. Phys. Chem. A*, 2014, **118**, 1673–1683.
136 D. Du, H. Fliegl and D. Sundholm, *J. Chin. Chem. Soc.*, 2016, **63**, 93–100.
137 P. W. Atkins and R. S. Friedman, *Molecular Quantum Mechanics*, Oxford University Press, 1997.
138 J. Jusélius, D. Sundholm and J. Gauss, *J. Chem. Phys.*, 2004, **121**, 3952–3963.
139 S. Taubert, D. Sundholm and J. Jusélius, *J. Chem. Phys.*, 2011, **134**, 054123:1–12.
140 PyNgl: Scientific visualization Python program package, http://www.pyngl.ucar.edu.
141 J. Ahrens, B. Geveci, C. Law, *ParaView: An End-User Tool for Large Data Visualization, Visualization Handbook*, Elsevier, 2005, ISBN-13: 978-0123875822, see also: http://www.paraview.org.
142 GIMIC, version 2.0, a current density program, Can be freely downloaded from https://github.com/qmcurrents/gimic.
143 C. Kumar, H. Fliegl and D. Sundholm, *J. Phys. Chem. A*, 2017, **121**, 7282–7289.
144 K. Ruud, H. Skaane, T. Helgaker, K. L. Bak and P. Jørgensen, *J. Am. Chem. Soc.*, 1994, **116**, 10135–10140.
145 R. F. W. Bader and T. A. Keith, *J. Chem. Phys.*, 1993, **99**, 3683–3693.
146 P. Pascal, *Ann. Chim. Phys.*, 1910, **19**, 5–70.
147 A. Pacault, *Rev. Sci.*, 1948, **86**, 38–61.
148 P. Pascal, F. Gallais and S. F. C. R. Labarre, *C. R. Acad. Sci.*, 1961, **252**, 2644–2649.
149 K. Ruud, T. Helgaker, K. L. Bak, P. Jørgensen and H. J. A. Jensen, *J. Chem. Phys.*, 1993, **99**, 3847–3859.
150 J. Jusélius and D. Sundholm, *J. Org. Chem.*, 2000, **65**, 5233–5237.
151 E. Steiner, P. W. Fowler and R. W. A. Havenith, *J. Phys. Chem. A*, 2002, **106**, 7048–7056.
152 E. Steiner, A. Soncini and P. W. Fowler, *Org. Biomol. Chem.*, 2005, **4**, 4053–4059.
153 J.-I. Aihara, E. Kimura and T. M. Krygowski, *Bull. Chem. Soc. Jpn.*, 2008, **81**, 826–835.
154 J.-I. Aihara, *J. Phys. Chem. A*, 2008, **112**, 5305–5311.
155 M. Bröring, *Angew. Chem., Int. Ed.*, 2011, **50**, 2436–2438.
156 J. I. Wu, I. Fernández and P. von Ragué Schleyer, *J. Am. Chem. Soc.*, 2013, **135**, 315–321.
157 M. Stepień and L. Latos-Grażyński, *Aromaticity in Heterocyclic Compounds*, Springer, Berlin, Heidelberg, 2009, vol. 19, pp. 83–153.
158 J. Aihara and M. Makino, *Org. Biomol. Chem.*, 2010, **8**, 261–266.

159 E. Steiner and P. W. Fowler, *Org. Biomol. Chem.*, 2004, **2**, 34–37.
160 J. Ren, F.-Q. Bai and H.-X. Zhang, *Int. J. Quantum Chem.*, 2015, **115**, 983–988.
161 E. Steiner and P. W. Fowler, *Org. Biomol. Chem.*, 2002, **3**, 114–116.
162 E. Steiner and P. W. Fowler, *Org. Biomol. Chem.*, 2006, **4**, 2473–2476.
163 E. Steiner, P. W. Fowler, A. Soncini and L. W. Jenneskens, *Faraday Discuss.*, 2007, **135**, 309–323.
164 R. Carion, B. Champagne, G. Monaco, R. Zanasi, S. Pelloni and P. Lazzeretti, *J. Chem. Theory Comput.*, 2010, **6**, 2002–2018.
165 G. Monaco, R. Zanasi, S. Pelloni and P. Lazzeretti, *J. Chem. Theory Comput.*, 2010, **6**, 3343–3351.
166 P. W. Fowler, M. Lillington and L. P. Olson, *Pure Appl. Chem.*, 2007, **79**, 969–979.
167 P. Fowler, R. Zanasi, B. Cadioli and E. Steiner, *Chem. Phys. Lett.*, 1996, **251**, 132–140.
168 E. Vogel, W. Haas, B. Knipp, J. Lex and H. Schmickler, *Angew. Chem., Int. Ed.*, 1988, **27**, 406–409.
169 E. Vogel, *J. Heterocycl. Chem.*, 1996, **33**, 1461–1487.
170 T. D. Lash, J. L. Romanic, J. Hayes and J. D. Spence, *Chem. Commun.*, 1999, 819–820.
171 L. E. Webb and E. B. Fleischer, *J. Am. Chem. Soc.*, 1965, **87**, 667–669.
172 N. C. Baird, *J. Am. Chem. Soc.*, 1972, **94**, 4941–4948.
173 J. S. Reddy and V. G. Anand, *J. Am. Chem. Soc.*, 2008, **130**, 3718–3719.
174 R. R. Valiev, H. Fliegl and D. Sundholm, *Chem. Commun.*, 2017, **53**, 9866–9869.
175 S. Grimme, *J. Comput. Chem.*, 2006, **27**, 1787–1799.
176 B. Szyszko, L. Latos-Grażyński and L. Szterenberg, *Angew. Chem., Int. Ed.*, 2011, **50**, 6587–6591.
177 T. D. Lash, M. J. Hayes, J. D. Spence, M. A. Muckey, G. M. Ferrence and L. F. Szczepura, *J. Org. Chem.*, 2002, **67**, 4860–4874.
178 D. I. AbuSalim and T. D. Lash, *J. Org. Chem.*, 2013, **78**, 11535–11548.
179 A. Ghosh, *Angew. Chem., Int. Ed.*, 2004, **43**, 1918–1931.
180 Y. Mitsushige, S. Yamaguchi, B. S. Lee, Y. M. Sung, S. Kuhri, C. A. Schierl, D. M. Guldi, D. Kim and Y. Matsuo, *J. Am. Chem. Soc.*, 2012, **134**, 16540–16543.
181 H. Fliegl, N. Özcan, R. Mera-Adasme, F. Pichierri, J. Jusélius and D. Sundholm, *Mol. Phys.*, 2013, **111**, 1364–1372.
182 Y. Chang, H. Chen, Z. Zhou, Y. Zhang, C. Schütt, R. Herges and Z. Shen, *Angew. Chem., Int. Ed.*, 2012, **51**, 12801–12805.
183 T. D. Lash, *Angew. Chem., Int. Ed.*, 1995, **34**, 2533–2535.
184 T. D. Lash, M. J. Hayes, J. D. Spence, M. A. Muckey, G. M. Ferrence and L. F. Szczepura, *J. Org. Chem.*, 2002, **67**, 4860–4874.
185 D. I. AbuSalim and T. D. Lash, *Org. Biomol. Chem.*, 2014, **12**, 8719–8736.
186 T. D. Lash and M. J. J. Hayes, *Angew. Chem., Int. Ed.*, 1997, **36**, 840–842.
187 T. D. Lash, S. T. Chaney and D. T. Richter, *J. Org. Chem.*, 1998, **63**, 9076–9088.
188 S. R. Graham, D. A. Colby and T. D. Lash, *Angew. Chem., Int. Ed.*, 2002, **41**, 1371–1374.
189 T. D. Lash, D. A. Colby, S. R. Graham and S. T. Chaney, *J. Org. Chem.*, 2004, **69**, 8851–8864.
190 K. M. Bergman, G. M. Ferrence and T. D. Lash, *J. Org. Chem.*, 2004, **69**, 7888–7897.
191 T. D. Lash and S. T. Chaney, *Tetrahedron Lett.*, 1996, **37**, 8825–8828.
192 D. Li and T. D. Lash, *J. Org. Chem.*, 2014, **79**, 7112–7121.

193 D. Andrae, U. Häussermann, M. Dolg, H. Stoll and H. Preuss, *Theor. Chim. Acta*, 1990, **77**, 123–141.
194 U. Wahlgren, *European Summer School in Quantum Chemistry*, Lund Universitet, 2000, vol. 3, pp. 599–639.
195 M. Rauhalahti, S. Taubert, D. Sundholm and V. Liegeois, *Phys. Chem. Chem. Phys.*, 2017, **19**, 7124–7131.
196 D. Sulzer, M. Olejniczak, R. Bast and T. Saue, *Phys. Chem. Chem. Phys.*, 2011, **13**, 20682–20689.
197 R. Bast, J. Jusélius and T. Saue, *Chem. Phys.*, 2009, **356**, 187–194.
198 R. J. F. Berger, M. Repisky and S. Komorovsky, *Chem. Commun.*, 2015, **51**, 13961–13963.
199 S. Hiramatsu, S. Sugawara, S. Kojima and Y. Yamamoto, *J. Porphyrins Phalocyanines*, 2013, **17**, 1–5.
200 R. Nozawa, K. Yamamoto, J. Shin, S. Hiroto and H. Shinokubo, *Angew. Chem., Int. Ed.*, 2015, **54**, 8454–8457.
201 R. Nozawa, K. Yamamoto, I. Hisaki, J. Shina and H. Shinokubo, *Chem. Commun.*, 2016, **52**, 7106–7109.
202 H. Fliegl, 2017, unpublished.
203 Y. J. Franzke, D. Sundholm and F. Weigend, *Phys. Chem. Chem. Phys.*, 2017, **19**, 12794–12803.
204 D. Ajami, O. Oeckler, A. Simon and R. Herges, *Nature*, 2003, **426**, 819–821.
205 D. Ajami, K. Hess, F. Köhler, C. Näther, O. Oeckler, A. Simon, C. Yamamoto, Y. Okamoto and R. Herges, *Chem. – Eur. J.*, 2006, **12**, 5434–5445.
206 S. Taubert, D. Sundholm and F. Pichierri, *J. Org. Chem.*, 2009, **74**, 6495–6502.
207 E. Heilbronner, *Tetrahedron Lett.*, 1964, **5**, 1923–1928.
208 S. Shimizu, N. Aratani and A. Osuka, *Chem. – Eur. J.*, 2006, **12**, 4909–4918.
209 V. J. Bauer, D. L. J. Clive, D. Dolphin and J. B. Paine III, *J. Am. Chem. Soc.*, 1983, **105**, 6429–6436.
210 J. Setsune and S. Maeda, *J. Am. Chem. Soc.*, 2000, **122**, 12405–12406.
211 J. Y. Shin, H. Furuta, S. Igarashi and A. Osuka, *J. Am. Chem. Soc.*, 2001, **123**, 7190–7191.
212 N. Sprutta and L. Latos-Grażyński, *Chem. – Eur. J.*, 2001, **7**, 5099–5112.
213 J. Setsune, Y. Katakami and N. Iizuna, *J. Am. Chem. Soc.*, 1999, **121**, 8957–8958.
214 J. Sankar, S. Mori, S. Saito, H. Rath, M. Suzuki, Y. Inokuma, H. Shinokubo, K. S. Kim, Z. S. Yoon, J. Y. Shin, J. M. Lim, Y. Matsuzaki, O. Matsushita, A. Muranaka, N. Kobayashi, D. Kim and A. Osuka, *J. Am. Chem. Soc.*, 2008, **130**, 13568–13579.
215 N. Jux, *Angew. Chem., Int. Ed.*, 2008, **47**, 2543–2546.
216 J.-Y. Shin, K. S. Kim, M.-C. Yoon, J. M. Lim, Z. S. Yoon, A. Osuka and D. Kim, *Chem. Soc. Rev.*, 2010, **39**, 2751–2767.
217 A. Osuka and S. Saito, *Chem. Commun.*, 2011, **47**, 4330–4339.
218 Z. S. Yoon, A. Osuka and D. Kim, *Nat. Chem.*, 2009, **1**, 113–122.
219 Y. Tanaka, S. Saito, S. Mori, N. Aratani, H. Shinokubo, N. Shibata, Y. Higuchi, Z. S. Yoon, K. S. Kim, S. B. Noh, J. K. Park, D. Kim and A. Osuka, *Angew. Chem., Int. Ed.*, 2008, **47**, 681–684.
220 M. Stepień, B. Szyszko and L. Latos-Grażyński, *Org. Lett.*, 2009, **11**, 3930–3933.
221 M. Stepień, L. Latos-Grażyński, N. Sprutta, P. Chwalisz and L. Szterenberg, *Angew. Chem., Int. Ed.*, 2007, **46**, 7869–7873.
222 J.-Y. Shin, K. S. Kim, M.-C. Yoon, J. M. Lim, Z. S. Yoon, A. Osuka and D. Kim, *Chem. Soc. Rev.*, 2010, **39**, 2751–2767.

223 S. Saito, J. Y. Shin, J. M. Lim, K. S. Kim, D. Kim and A. Osuka, *Angew. Chem., Int. Ed.*, 2008, **47**, 9657–9660.
224 T. Higashino, J. M. Lim, T. Miura, S. Saito, J.-Y. Shin, D. Kim and A. Osuka, *Angew. Chem., Int. Ed.*, 2010, **49**, 1–6.
225 T. Higashino and A. Osuka, *Chem. Sci.*, 2013, **4**, 1087–1091.
226 K. Naoda and A. Osuka, *Asian J. Org. Chem.*, 2017, **6**, 1205–1208.
227 C. S. M. Allan and H. S. Rzepa, *J. Org. Chem.*, 2008, **73**, 6615–6622.
228 C. S. M. Allan and H. S. Rzepa, *J. Chem. Theory Comput.*, 2008, **4**, 1841–1848.
229 H. Fliegl, D. Sundholm and F. Pichierri, *Phys. Chem. Chem. Phys.*, 2011, **13**, 20659–20665.
230 H. S. Rzepa, *Org. Lett.*, 2008, **10**, 949–952.
231 S. M. Rappaport and H. S. Rzepa, *J. Am. Chem. Soc.*, 2008, **130**, 7613–7619.
232 G. Călugăreanu, *Czech. Math. J.*, 1961, **11**, 588–625.
233 W. F. Pohl, *Indiana Univ. Math. J.*, 1968, **17**, 975–985.
234 J. H. White, *Am. J. Math.*, 1969, **91**, 693–728.
235 F. B. Fuller, *Proc. Natl. Acad. Sci. U. S. A.*, 1971, **68**, 815–819.
236 C. S. Wannere, H. S. Rzepa, B. C. Rinderspacher, A. Paul, C. S. M. Allan, H. F. Schaefer III and P. von Ragué Schleyer, *J. Phys. Chem. A*, 2009, **113**, 11619–11629.
237 M. Stepień, N. Sprutta and L. Latos-Grażyński, *Angew. Chem., Int. Ed.*, 2011, **50**, 4288–4340.
238 T. Soya, K. Naoda and A. Osuka, *Chem. – Asian J.*, 2015, **10**, 231–238.
239 M. Ishida, T. Furuyama, J. M. Lim, S. Lee, Z. Zhang, S. K. Ghosh, V. M. Lynch, C.-H. Lee, N. Kobayashi, D. Kim and J. L. Sessler, *Chem. – Eur. J.*, 2017, **23**, 6682–6692.
240 S.-I. Ishida, J. O. Kim, D. Kim and A. Osuka, *Chem. – Eur. J.*, 2016, **22**, 16554–16561.
241 T. Yoneda, Y. M. Sung, J. M. Lim, D. Kim and A. Osuka, *Angew. Chem., Int. Ed.*, 2014, **53**, 13169–13173.
242 K. S. Anju, M. Das, B. Adinarayana, C. H. Suresh and A. Srinivasan, *Angew. Chem., Int. Ed.*, 2017, **56**, 15667–15671.
243 T. Soya, H. Mori, Y. Hong, Y. H. Koo, D. Kim and A. Osuka, *Angew. Chem., Int. Ed.*, 2017, **56**, 3232–3236.
244 M. Izawa, T. Kim, S.-I. Ishida, T. Tanaka, T. Mori, D. Kim and A. Osuka, *Angew. Chem., Int. Ed.*, 2017, **56**, 3982–3986.
245 T. Higashino, T. Soya, W. Kim, D. Kim and A. Osuka, *Angew. Chem., Int. Ed.*, 2015, **54**, 5456–5459.
246 G. R. Schaller and R. Herges, *Chem. Commun.*, 2012, **49**, 1254–1260.
247 D. Ajami, O. Oeckler, R. A. Simon and R. Herges, *Nature*, 2003, **426**, 819–821.
248 R. Herges, *Chem. Rev.*, 2006, **106**, 4820–4842.
249 C. Castro, Z. Chen, C. S. Wannere, H. Jiao, W. L. Karney, M. Mauksch, R. Puchta, N. J. R. van Eikema Hommes and P. von Ragué Schleyer, *J. Am. Chem. Soc.*, 2005, **127**, 2425–2432.
250 M. Pawlicki, K. Hurej, L. Szterenberg and L. Latos-Grażyński, *Angew. Chem., Int. Ed.*, 2014, **53**, 2992–2996.
251 A. Osuka, E. Tsurumaki and T. Tanaka, *Bull. Chem. Soc. Jpn.*, 2011, **84**, 679–697.
252 Y. Inokuma and A. Osuka, *Dalton Trans.*, 2008, 2517–2526.
253 E. Tsurumaki, J. Sung, D. Kim and A. Osuka, *J. Am. Chem. Soc.*, 2015, **137**, 1056–1059.
254 C. Azarias, M. Pawelek and D. Jacquemin, *J. Phys. Chem. A*, 2017, **121**, 4306–4317.
255 F. Pichierri, *Chem. Phys. Lett.*, 2006, **426**, 410–414.

256 P. Campomanes, M. I. Menendez, G. I. Cardenas-Jiron and T. L. Sordo, *Phys. Chem. Chem. Phys.*, 2007, **9**, 5644–5648.
257 J. H. van Vleck, *The Theory of Electric and Magnetic Susceptibilities*, Oxford University Press, London, 1932, pp. 1–384.
258 R. A. Hegstrom and W. N. Lipscomb, *Rev. Mod. Phys.*, 1968, **40**, 354–358.
259 P. W. Fowler and E. Steiner, *Mol. Phys.*, 1991, **74**, 1147–1158.
260 S. P. A. Sauer, T. Enevoldsen and J. Oddershede, *J. Chem. Phys.*, 1993, **98**, 9748–1158.
261 K. Ruud, T. Helgaker, K. L. Bak, P. Jørgensen and J. Olsen, *Chem. Phys.*, 1995, **195**, 157–169.
262 R. R. Valiev, H. Fliegl and D. Sundholm, *Phys. Chem. Chem. Phys.*, 2017, **19**, 25979–25988.
263 O. Christiansen, H. Koch and P. Jørgensen, *Chem. Phys. Lett.*, 1995, **243**, 409–418.
264 C. Hättig and A. Köhn, *J. Chem. Phys.*, 2002, **117**, 6939–6951.
265 C. Hättig, *Adv. Quantum Chem.*, 2005, **50**, 37–60.
266 G. V. Baryshnikov, R. R. Valiev, N. N. Karaush and B. F. Minaev, *Phys. Chem. Chem. Phys.*, 2014, **16**, 15367–15374.
267 G. V. Baryshnikov, N. N. Karaush, R. R. Valiev and B. F. Minaev, *J. Mol. Model.*, 2015, **21**, 136.
268 G. V. Baryshnikov, R. R. Valiev, N. N. Karaush, D. Sundholm and B. F. Minaev, *Phys. Chem. Chem. Phys.*, 2016, **18**, 8980–8992.
269 C. Kumar, T. Kjærgaard, T. Helgaker and H. Fliegl, *J. Chem. Phys.*, 2016, **145**, 234108.